Research Report 2015–05

High-resolution gridded data generation and performance assessment of multiple statistical downscaling methods for South Korea

Hyung–Il Eum

APCC
APEC CLIMATE CENTER

Research Report 2015–05

High-resolution gridded data generation and performance assessment of multiple statistical downscaling methods for South Korea

Hyung–Il Eum

APCC
APEC CLIMATE CENTER

PREFACE

As state-of-the-art techniques have advanced Atmosphere-Ocean General Circulation Models (AOGCMs) and Regional Circulation Models (RCMs), demands for long-term high-resolution climate data in the form of regularly spaced grid cells have also increased to directly compare the skill of RCMs within a domain. The spatial resolution of statistical downscaling methods corresponds to the resolution of observational data, where spatial climate data is created by a process of statistically interpolating observational station data. Spatial climate data is employed in statistical downscaling methods to provide a downscaled gridded climate data set for applications at regional or local scales, such as ecological and hydrologic impact studies. In this study, a long-term gridded climate data set was generated over South Korea using an Improved GIS-based Regression Model (IGISRM) which considers the density of stations near each grid cell.

APCC is very interested in providing the most accurate and relevant seamless forecasts given by a Multi-Model Ensemble (MME) system. Though MME has provided useful climate information, further processes may need to better capture regional climatology and to improve skills at finer scales. Therefore, development of statistical downscaling techniques is an essential direction towards APCC's goals. This study compared the performance of statistical downscaling methods, which have been widely used in various fields, based on a suite of performance metrics. The results showed that the four statistical downscaling methods considerably improved performances in reproducing distribution, spatial correlation, and extreme events.

This study also provided a reliable long-term gridded data set for calibration

and validation of climatic and hydrologic models and, based on the performance metrics suggested in this study, a guidance to select robust statistical downscaling methods. At APCC, the statistical downscaling technique may play an important role in improving the skill of MME at the regional scale for incorporating MME outputs into post-stages such as agricultural and water resources planning and management. Regarding this study, I acknowledge the dedicated work of Hyung-Il Eum and the support from colleagues and researchers at APCC.

Dr. **Chin-Seung Chung**, Director
APEC Climate Center
January 2016

ABSTRACT

As advances have been made in climate models and process-based land-surface schemes, the requirements of long-term high-resolution climate data for efficient modelling and performance assessment have also increased. Recently, long-term gridded climate data have been actively employed to produce high-resolution climate projections by using statistical downscaling methods because the spatial resolutions of statistical downscaling methods correspond to those of historical data. This study presents an improved geographic information system (GIS)-based regression model (IGISRM) that incorporates an adaptive effective radius algorithm into the structure of a previous regression model of Kongju National University (KNU/RM). Long-term gridded climate data from 1973 to 2010 are generated, and the performances of IGISRM at various spatial resolutions are evaluated to identify the most suitable grid spacing with respect to accuracy and computational efficiency. In addition, inter-comparison of the performances of IGISRM and KNU/RM is conducted with multiple performance measures and extreme indices.

A number of statistical downscaling methodologies have been introduced to bridge the gap in scale between outputs of climate models and the climate information needed to assess potential impacts at local and regional scales. Four statistical downscaling methods—Bias-Correction/Spatial Disaggregation (BCSD), Bias-Correction/ Constructed Analog (BCCA), Multivariate Adaptive Constructed Analogs (MACA), and Bias-Correction/Climate Imprint (BCCI)—are applied to downscale the latest Climate Forecast System Reanalysis (CFSR) data to stations for precipitation (PRCP), maximum temperature (TMAX), and minimum temperature (TMIN) over South Korea.

All methods are calibrated with observational station data for 19 years from 1973 to 1991 and are tested for the recent 19 years from 1992 to 2010. A comprehensive suite of performance metrics is presented to inter-compare methods with respect to reproducing the sequencing of events and distribution of climate variables, spatial structure, and extremes. Based on the performance metrics, this study employs the Technique for Order of Preference by Similarity to Ideal Solution (TOPSIS) to identify a robust statistical downscaling method.

The results show that both regression models produce compatible performance measures for PRCP, TMAX, and TMIN. However, IGISRM outperforms the KNU/RM in reproducing spatial distribution of precipitation events, particularly when a considerable level of spatial variability occurs in precipitation events. On the contrary, KNU/RM overpredicts many wet days with very small amounts of precipitation, referred to as the drizzling effect. Such results indicate that IGISRM has better skill for capturing the spatial heterogeneity in precipitation occurrence. In addition, IGISRM shows higher skill in reproducing extreme indices, particularly those related to wet and dry spells of precipitation owing mainly to overpredicted wet days of KNU/RM induced by an overly long radius of the influence circle. Regarding the inter-comparison of statistical downscaling methods, the downscaling skill is considerably affected by the skill of the general circulation model (GCM; (i.e., CFSR in this study)), and all methods lead to large improvements in representing all performance metrics. BCSD and BCCI, employing the spatial disaggregation algorithm, show slightly better skill in reproducing distributions and extremes, whereas BCCA and MACA, incorporating spatial weather patterns, outperform BCSD and BCCI in reproducing spatial structures. All statistical downscaling methods show lower skill at higher elevations where climate extremes are influenced by orographic and complex topographic effects. When TOPSIS is applied to the comprehensive performance metrics, MACA is identified as the most reliable and

robust method for all variables, whereas BCCI shows the poorest performance owing mainly to lack of skill in simulating the spatial structure.

CONTENTS

1. INTRODUCTION

Global Climate Models (GCMs) are a primary tool not only to provide insight into global climate responses to natural and anthropogenic changes but also to assess the potential impacts of climate change on local hydrologic systems and water resources (Wood et al., 2004; Christensen and Lettenmairer, 2007; Maurer et al., 2010; Hay et al., 2014). Most climate change impact studies require fine-resolution input data sufficient to modeling and simulating climate-relevant problems at regional or local scales whereas GCMs provide climate information with coarse resolution, generally at a grid-spacing of $\sim$1°–2° (Olsson et al., 2001; Dibike and Coulibaly, 2006; Fowler et al., 2007). In addition, simulated outputs from global and regional climate models have shown considerable systematic biases with respect to observational datasets (Mearns et al., 2012; Sillmann et al., 2013) owing mainly to an unresolved sub-grid scale (Cherubini et al., 2002), physical parameterizations (Jenkins and Lowe, 2003; Mizuta et al., 2006), and cascade errors from boundary forcing in regional climate models (Deque et al., 2007; Christensen et al., 2007).

To provide relevant climate information at scales needed to assess local and regional impacts, downscaling techniques are often employed (Wilby et al., 1998; Haylock et al., 2006; Hidalgo et al., 2008; Abatzoglou and Brown, 2012; Stoner et al., 2013). Of the two main categories of downscaling, dynamical and statistical, prior studies have often applied statistical downscaling methods, which have advantages in computational efficiency and the ability to reproduce essential statistics of regional observed climate data (Bardossy et al., 2005; Haylock et al., 2006; Eum and Simonovic, 2012).

Recently, such as Bias-Correction/Spatial Disaggregation (BCSD; Wood et al., 2004), Bias-Correction/Constructed Analog (BCCA; Maurer et al., 2010), Multivariate Adaptive Constructed Analog (MACA; Abatzoglou and Brown, 2012), Bias-Correction/Stochastic Analog (BCSA; Hwang and Graham, 2013), Bias-Correction/Climate Imprint (BCCI; Hunter and Meetemeyer, 2005), Model Output Statistics (MOS)-based methods have been actively applied to downscale outputs of GCMs at local scales. As a result of the plethora of techniques, inter-comparison studies have been conducted to identify more robust downscaling methods with regard to extremes (Segui et al., 2010;

Goodess et al., 2012; Thrasher et al., 2012; Bürger et al., 2013), wildfire applications (Abatzoglou and Brown, 2012), and water resources assessment (Eum et al., 2010; Chen et al., 2011; Gutmann et al., 2014). Four statistical downscaling methods widely used in various fields—BCSD, BCCA, MACA, and BCCI—are selected in this study for inter-comparison of their performances on a suite of evaluation metrics.

High-resolution climate data in the form of regularly spaced grid cells are very useful for direct comparison of the performance of Regional Climate Models (RCMs) with the gridded dataset at all grid cells within a domain. Because the spatial resolution of the statistical downscaling methods corresponds to the resolution of observational data, spatial climate data created by a process of statistical interpolation of observational station data have also been employed in statistical downscaling methods. This technique is used to provide a downscaled gridded climate dataset with a finer spatial resolution from GCM outputs for regional or local-scale applications such as ecological and hydrologic impact studies (Brekke et al., 2009; Barsugli et al., 2013; Hanson et al., 2012, Miller et al., 2013; Werner et al., 2013; Gutmann et al., 2014; Hay et al., 2014). Gridded precipitation and temperature datasets at 5 km spatial resolution have been generated with the Parameter-Elevation Regressions on Independent Slopes Model (PRISM) structure based on 526 stations in South Korea (Hong et al., 2007; Shin et al., 2008). Kongju National University (KNU) has improved the previous datasets in terms of spatial resolution and extension of the time window (Lee et al., 2014) in its KNU/Regression Model (KNU/RM), employing 526 station data. The Climate Change Information Center (CCIC) of the Korea Meteorological Administration (KMA) has recently employed the KNU/RM to generate high-resolution observational gridded climate data from 2001 to 2014 at 1 km resolution over South Korea (www.climate.go.kr). Because 450 of 526 stations, or 86%, have been installed as of 2001, the length of the observation period is not sufficient to uses of post applications such as hydrologic modeling and statistical downscaling that require long-term datasets for calibration and validation. Moreover, KNU/RM used a fixed radius of influence over a domain, which may cause an unexpected bias in the case of an excessively long radius of influence for a spatially strong heterogeneous region in climatology. Therefore, a long-term gridded climate dataset based on 60 stations with more than 30 years of observations is generated in the present study by using an Improved GIS-based Regression Model (IGISRM),

which combines the KNU/RM structure with the Daymet model by incorporating an iterative station density algorithm. That is, local regression is implemented on the basis of the PRISM structure in which the radius of influence varies with the density of the station at each grid cell. To validate the applicability of IGISRM, we compare its output with other station data not used in IGISRM for 2000 to 2010.

Formulating precise and informative evaluation metrics is a prerequisite for efficient completion of statistical downscaling inter-comparison. Murdock et al. (2013) evaluated statistical downscaling methods by using three diagnostics including sequencing of events, distribution of values, and spatial structure. Bürger et al. (2013) inter-compared multiple methods in terms of their ability to reproduce climate extreme indices recommended by the World Meteorological Organization's Expert Team on Climate Change Detection and Indices (ETCCDI; Zhang et al., 2011). Integrating all diagnostics employed in prior studies, I evaluate skill based on the following four criteria: 1) sequence of events (correlation between downscaled and observational datasets), 2) distribution of values the Kolmogorov–Smirnov D (K–S D) statistic, 3) spatial structure (spatial correlation between stations), and 4) ability to reproduce extreme events (K–S test for 23 ETCCDI indices). We use the Climate Forecast System Reanalysis (CFSR) version 2 (Saha et al., 2010) as a surrogate for a climate model, which places more focus on the skill of methods than on the fidelity of one or more climate models (Wilby et al., 2000; Fasbender and Ouarda, 2010; Nicholas and Battisti, 2012).

In prior studies, downscaling methods have shown different levels of skill for different performance metrics. This generally makes selection of the most skillful method difficult and potentially ambiguous. As a branch of Multi-criteria Decision Making (MCDM), the Technique for Order of Preference by Similarity to Ideal Solution (TOPSIS), originally developed by Hwang and Yoon (1981), provides a tool for sorting alternatives that are simultaneously far from the worst solution and close to the best condition (Chu, 2002; Kim and Chung, 2014). By using the TOPSIS technique, an approach to rank methods based on the full suite of performance metrics is presented. The resulting rank may be informative for end-user to select the most suitable method in an available inventory.

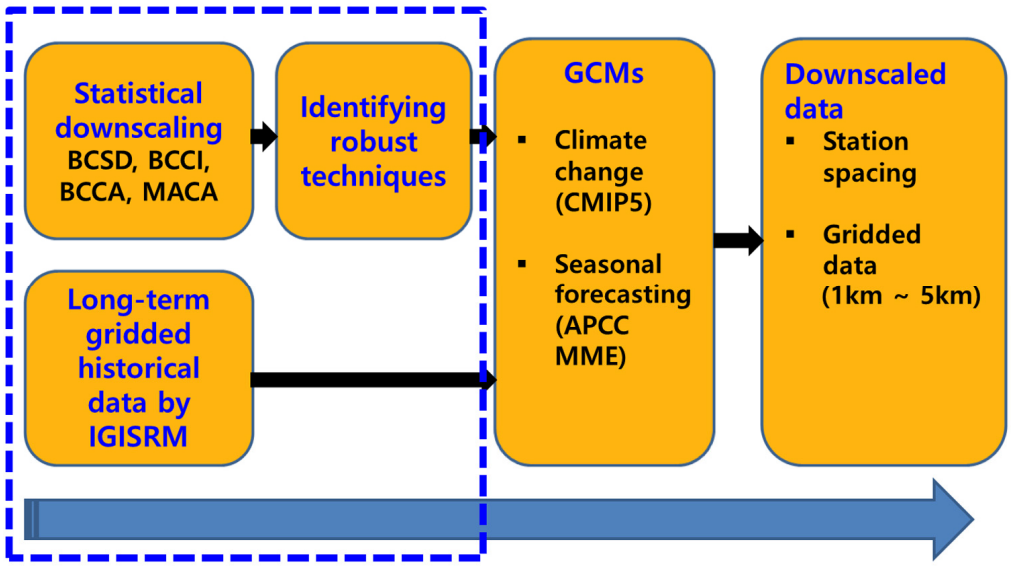

Figure 1.1 Schematic research plan and products

A schematic diagram of the research plan and corresponding products for this study is presented in Figure 1.1. The ultimate goals of this study are to downscale climate change scenarios and seasonal forecasting generated by GCMs at station and gridded data resolutions. Specifically, the focus in the current year is on 1) developing and applying the four statistical downscaling methods for South Korea, 2) inter-comparing the skill of each method on the four performance metrics, 3) ranking the methods by using the TOPSIS technique, and 4) developing the IGISRM method and generating a long-term gridded daily climate dataset over South Korea.

2. PRACTICAL APPLICATIONS OF STATISTICAL DOWNSCALING METHODS

2.1 Coordinated Regional Climate Downscaling Experiment

As a part of the activities of the EU-funded Ensemble-Based Predictions of Climate Changes and their Impacts (ENSEMBLES) project, a statistical downscaling portal was initiated, as shown in Figure 2.1. This portal provides interactive user-friendly tools to ease the downscaling process, which consists of four steps (Figure 2.2): 1) defining the predictors, 2) choosing the local/regional target variables to be downscaled, 3) defining the downscaling method, and 4) downscaling GCMs (Gutiérrez et al., 2012).

In predictor tab, the user can select predictors among commonly-used predictor variables (Table 2.1) in which available predictors vary with reanalysis datasets available within a selected target region. With combination of selected predictors, users need to select a predictand from the observed datasets. If there is no observed dataset within a user-selected region, the downscaling process cannot proceed further. The next step is to define the downscaling from non-generative (algorithmic) and generative (model-based) techniques provided by the portal (Figure 2.3). The non-generative technique includes two different types, analog and weather; the generative technique consists of linear regression, generalized linear model, and neural networks. Among these techniques, the user can test and validate with predictors and predictand selected to formulate the downscaling model. Once the predictor–predictand–downscaling method chain process has been completed, the final procedure is to downscale the GCM projections in the downscaling window (Figure 2.4).

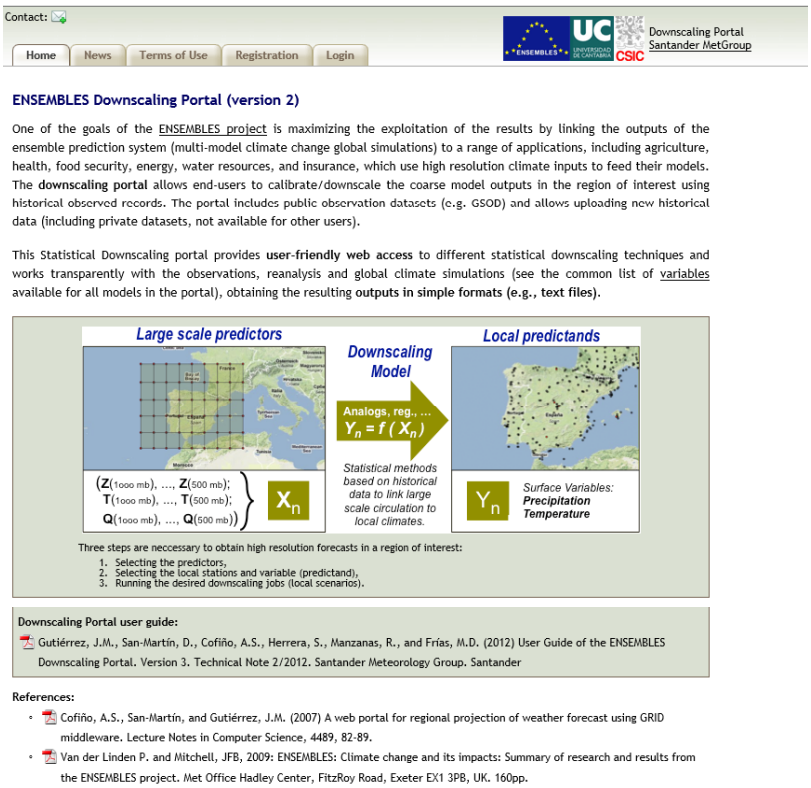

Figure 2.1 Ensemble-Based Predictions of Climate Changes and their Impacts (ENSEMBLES) downscaling portal (https://www.meteo.unican.es/downscaling/ensembles)

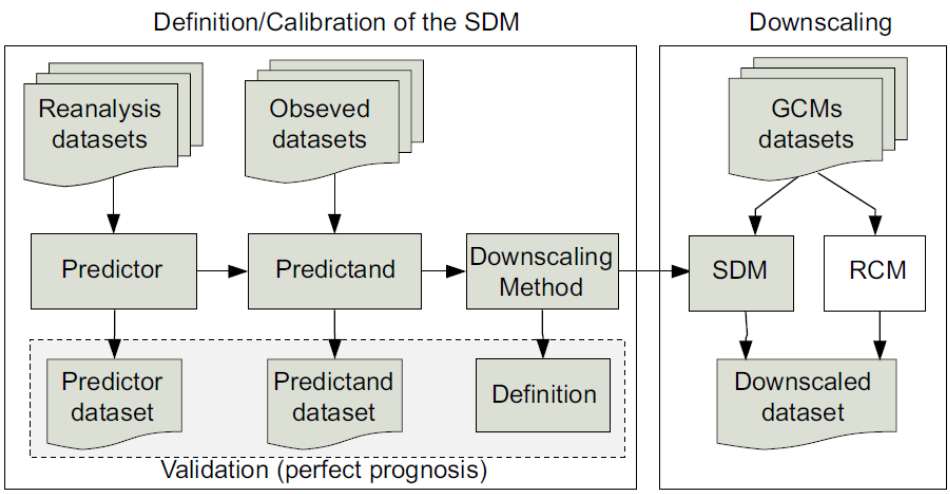

Figure 2.2 Schematic flow chart for the downscaling process (Gutiérrez et al., 2012)

Table 2.1 List of commonly used predictors in the downscaling portal

Variable	Levels (mb)
Geopotential	250, 500, 700, 850, 1000
Temperature	250, 500, 700, 850, 1000
U velocity	250, 500, 700, 850, 1000
V velocity	250, 500, 700, 850, 1000
Specific humidity	250, 500, 700, 850, 1000
2 m temperature	Surface
Mean sea level pressure	Surface
Maximum temperature	Surface
Minimum temperature	Surface
Total precipitation	Surface

(a) Non-generative (algorithmic) technique window

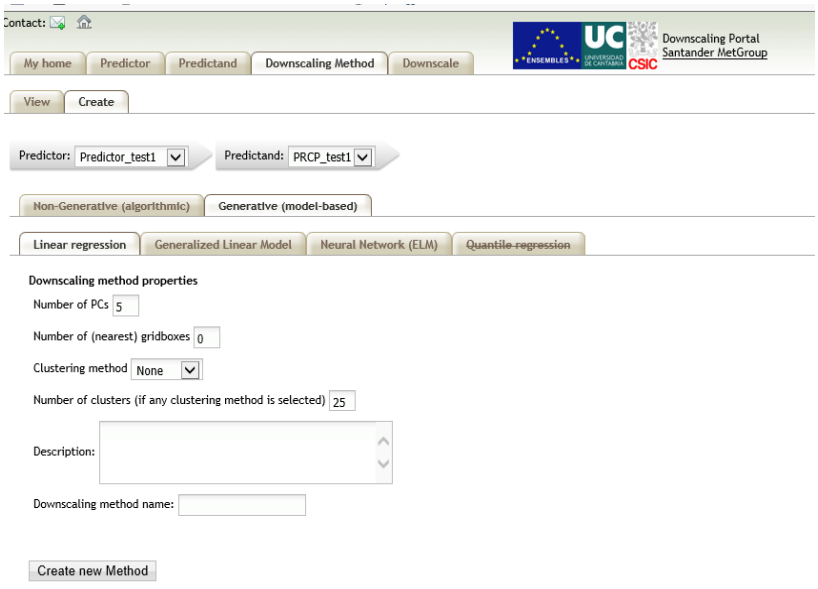

(b) Generative (model-based) technique window

Figure 2.3 Configuration panels of statistical downscaling methods

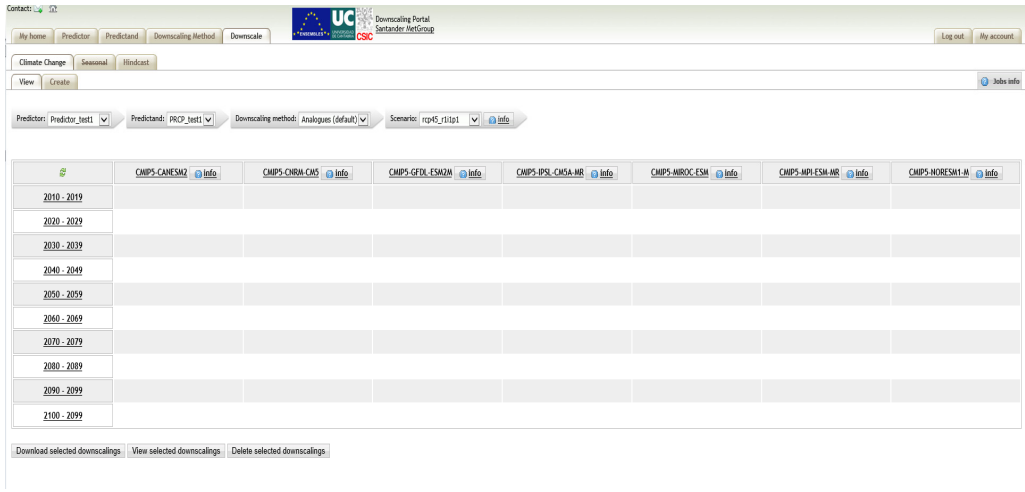

Figure 2.4 Snapshot of downscale window for generating downscaled GCM scenarios. Currently seven Coupled Model Inter-comparison Project Phase 5 (CMIP5) scenarios are available at the downscaling portal: CANESM2, CNRM-CM5, GFDL-ESM2M, IPSL-CM5A-MR, MIROC-ESM, MPI-ESM-MR, and NORESM1-M.

2.2 NASA Earth Exchange Global Daily Downscaled Projections

The National Aeronautics and Space Administration (NASA) Earth Exchange Global Daily Downscaled Projections (NEX-GDDP) dataset (Figure 2.5) provides downscaled climate scenarios worldwide for studies of climate change impacts. All data were derived from 21 GCM runs conducted under CMIP5 based on Representative Concentration Pathway (RCP)4.5 and RCP8.5 (Table 2.2). Each of the climate projections includes daily maximum temperature, minimum temperature, and precipitation for the period 1950–2100 at 0.25° (25 km × 25 km) spatial resolution.

By using a climate dataset from the Global Meteorological Forcing Dataset (GMFD) for Land Surface Modeling, available from the Terrestrial Hydrology Research Group at Princeton University [Sheffield et al., 2006], BCSD was applied to 42 downscaled GCM projections (21 GCMs × 2 RCPs) for daily maximum temperature, daily minimum temperature, and daily precipitation. The NEX-GDDP dataset was provided to assist the science community in conducting studies of climate change impacts at local to regional scales and to enhance public understanding of possible future global climate patterns at the spatial scales of individual towns, cities, and watersheds (Thrasher et al., 2012).

As an extended version of the GDDP data set, Thrasher et al. (2013) generated NEX-DCP30, a new archive of downscaled CMIP5 climate projections for the conterminous United States (U.S.) at 30-arc-second (~800 m) spatial resolution. This dataset is distributed through the NASA Center for Climate Simulations (NCCS) to support scientific analyses of regional climate change impacts and to provide informative climate projections for natural resources mangers in the U.S. As the observational climate set, the PRISM dataset developed at Oregon State University (Daly et al., 1994) was employed in combination with BCSD to provide high-resolution, bias-corrected climate projections. Figure 2.6 shows an example of climate change studies using NEX-DCP30 for the changes in springtime mean temperature from 1950 to 2099.

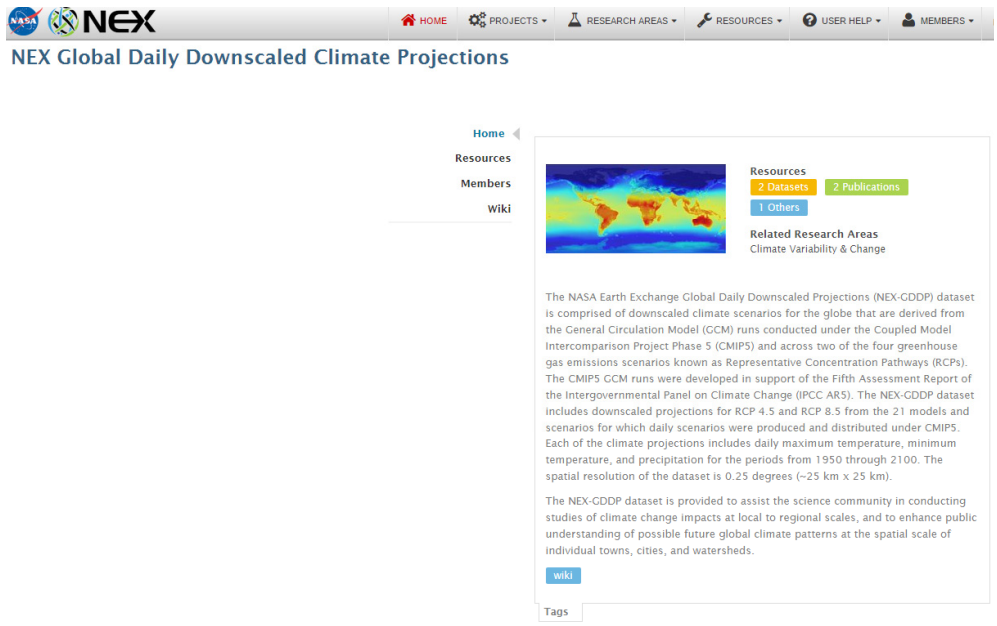

Figure 2.5 Snapshot of National Aeronautics and Space Administration Earth Exchange (NEX) Global Daily Downscaled Climate Projections (https://nex. nasa.gov/nex/projects/1356/)

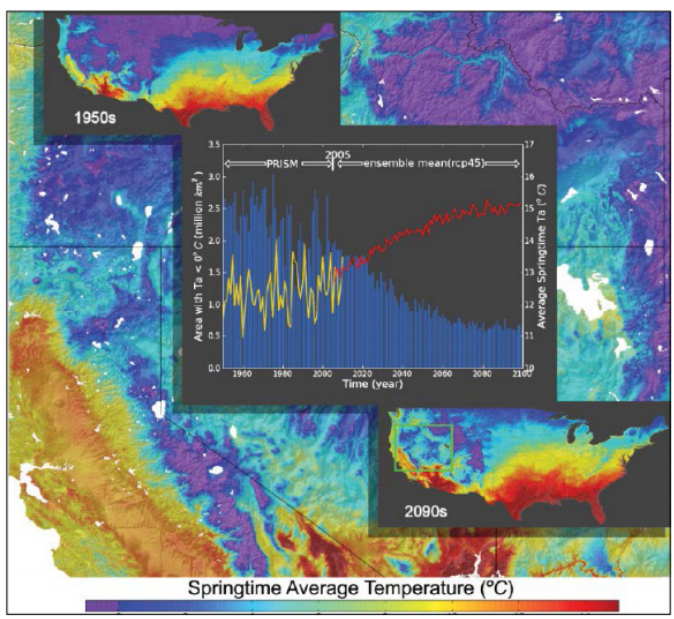

Figure 2.6 Changes in springtime mean temperature over the conterminous United States from 1950 to 2099

Table 2.2 Coupled Model Inter-comparison Project Phase 5 (CMIP5) models available as National Aeronautics and Space Administration (NASA) Earth Exchange Global Daily Downscaled Projections (NEX-GDDP) datasets

No	Model	Institution	Resolution Lon. × Lat.
1	BCC-CSM1-1	BCC	2.81° × 2.81°
2	CanESM2	CCCma	2.81° × 2.81°
3	CCSM4	NCAR	1.25° × 0.94°
4	CESM1-BGC	NCAR	1.25° × 0.94°
5	CNRM-CM5	CNRM-CERFACS	1.41° × 1.41°
6	GFDL-CM3	NOAA GFDL	2.50° × 2.00°
7	GFDL-ESM2G	NOAA GFDL	2.50° × 2.00°
8	GFDL-ESM2M	NOAA GFDL	2.50° × 2.00°
9	INM-CM4	INM	2.00° × 1.50°
10	IPSL-CM5A-LR	IPSL	3.75° × 1.88°
11	IPSL-CM5A-MR	IPSL	1.25° × 1.25°
12	MIROC5	AORI	1.41° × 1.41°
13	MIROC-ESM	JAMSTEC, AORI, NIES	2.81° × 2.81°
14	MIROC-ESM-CHEM	JAMSTEC, AORI, NIES	2.81° × 2.81°
15	MPI-ESM-LR	MPI-M	1.88° × 1.88°
16	MPI-ESM-MR	MPI-M	1.88° × 1.88°
17	MRI-CGCM3	MRI	1.13° × 2.25°
18	NorESM1-M	NCC	2.50° × 1.88°
19	ACCESS1-0	CAWCR	1.88° × 1.25°
20	BNU-ESM	BNU	2.81° × 2.81°
21	CSIRO-MK3-6-0	CSIRO	1.90° × 1.90°

2.3 Indian Ocean Climate Initiative Stage 3: Downscaled climate projections for Western Australia

The Commonwealth Scientific and Industrial Research Organization (CSIRO) has initiated the CSIRO Data Access Portal to provide access to data published by CSIRO. IOCI3, a climate research collaboration of CSIRO, Bureau of Meteorology (BoM), and the Government of Western Australia (WA), produced statistically downscaled projections for daily rainfall and maximum and minimum temperature for WA (Figure 2.7) using 29 sites for southwest WA and 19 for northwest WA including 9 in Kimberley 10 in Pilbara. The fine-scale projections for mid-century, 2047–2064, and end-of-century, 2082–2099, are provided in a user-friendly format of comma-separated-values (CSV) files to support scientific analyses of regional climate change impacts.

These statistically downscaled rainfall simulations were produced by using atmospheric predictors extracted from the historically based record using National Centers for Environmental Prediction/National Center for Atmospheric Research (NCEP/NCAR) reanalysis (NNR) for 1959–2009 and four GCMs including GFDL2.0, MIROC3.2, CSIRO-MK3.5, and MPI-ECHAM5 for the SRES B1 (low), A1B (medium) and A2 (high) greenhouse gas emissions scenarios. The NNR and GCM predictors were used to drive non-homogeneous Hidden Markov Models (NHMMs), which is a stochastic technique for generating multiple realizations of rainfall and temperature. The application of these techniques was advanced under IOCI3 and was applied to the tropics for the first time.

2.4 Northwest Climate Science Center Project in the U.S.: Integrated Scenarios of the Pacific Northwest, U.S.

The goal of the Integrated Scenarios of the Future Northwest Environment project in the U.S. was to use the latest global climate models and state of the science models of vegetation and hydrology to describe as accurately as possible the latest findings on the Northwest's future climate, vegetation, and hydrology. By evaluating the capacity of each GCM against models for simulating the observed climate patterns in the Northwest region, researchers determined the best-performing models, which were downscaled at finer grids for use in hydrology and vegetation models.

Figure 2.7 Study domain for Indian Ocean Climate Initiative Stage 3 (IOCI3)

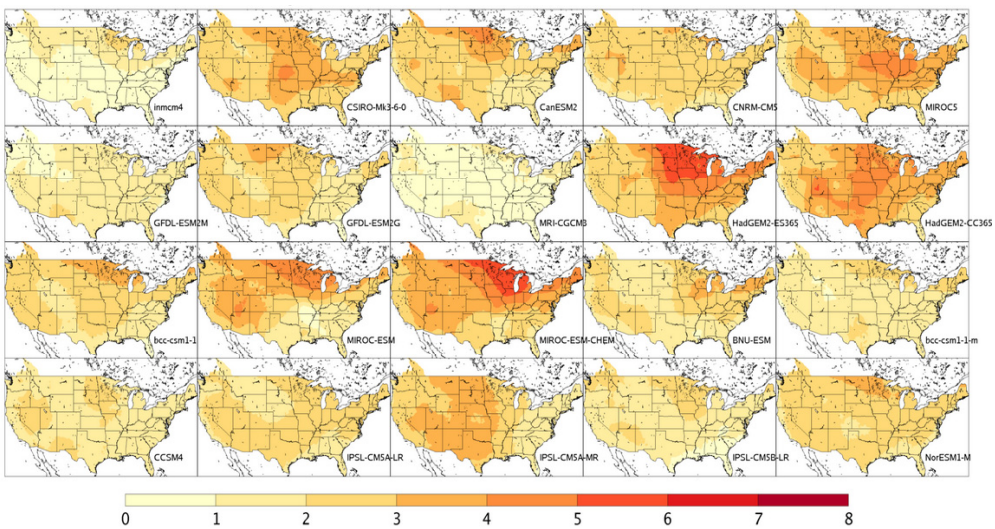

Figure 2.8 Changes in maximum temperature during the winter season of December–February between 2040–2069 and 1971–2000 for Representative Concentration Pathway (RCP)4.5 (http://climate.northwestknowledge.net/MACA/tool_projectionmaps.php)

The integrated scenarios team used a downscaling method known as the Multivariate Adaptive Constructed Analogs (MACA) to produce gridded data at 1/16° (~6 km), which was fine enough in detail to thoroughly model the region's topography (Figure 2.8). The downscaled gridded dataset was used as input data to the Variable Infiltration Capacity (VIC) model to provide gridded future hydrologic data for the western U.S. (Figure 2.9).

The products of this work are a series of freely available datasets that can be used to address specific management questions. These datasets are compatible with other hydrological and ecological modeling efforts and represent a next-generation climate change framework for land managers. This framework supports a range of management activities to increase the resilience of Northwest ecosystems, agricultural systems, and built environments. Moreover, it allows for the development of tools to help land managers identify the most vulnerable areas in the region and to develop strategies for reducing the impacts of climate change.

2.5 Downscaled CMIP3 and CMIP5 climate and hydrology projections

During 2012–2013, WCRP released global climate projections from CMIP5. Given the arrival of CMIP5 and how it differs from CMIP3, users were expected to show interest in this new information for local impact assessment and adaptation planning. This motivated the development of downscaled CMIP5 climate projections to enable users to compare this new information with the preceding downscaled CMIP3 information. Two statistical downscaling techniques, BCSD and BCCA, have been applied to CMIP5 projections for precipitation and maximum and minimum temperature (Figure 2.10) and are available at the Downscaled CMIP3 and CMIP5 Climate and Hydrology Projections (DCHP) http://gdo-dcp.ucllnl.org/downscaled_cmip_projections/. To date, hydrologic projection with BCSD is available at this website, where VIC applications have been developed for California, including the Klamath, Sacramento, and San Joaquin River basins; the Colorado River basin; the Great Basin, including the Truckee and Carson River basins; the Rio Grande; Missouri; the Pacific Northwest, including the Columbia River basin; Arkansas Red basin; and the Gulf of Mexico (Figure 2.11).

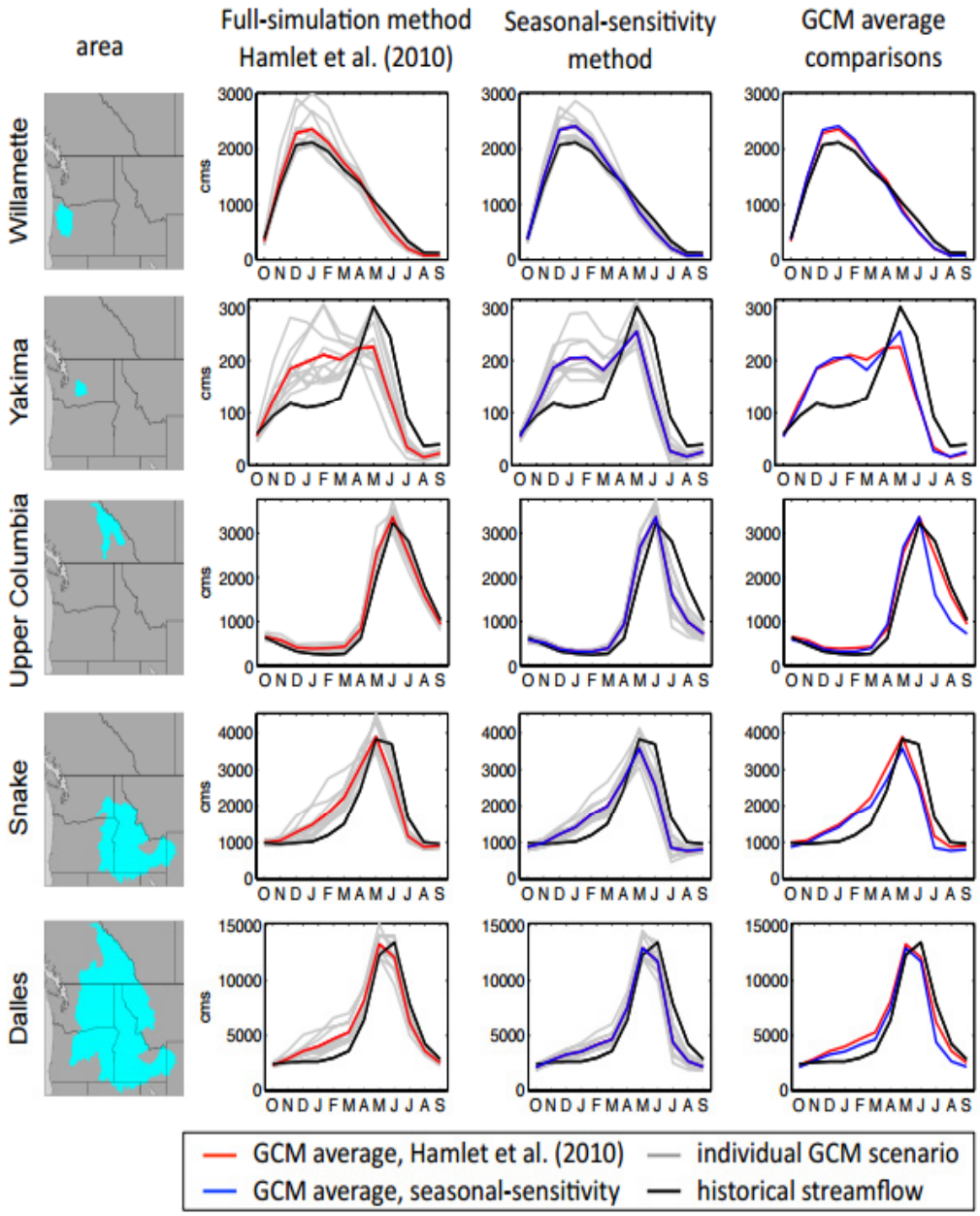

Figure 2.9 Comparison of monthly average streamflow projections for the 2040s at five locations throughout the Columbia River basin (Vano et al., 2015).

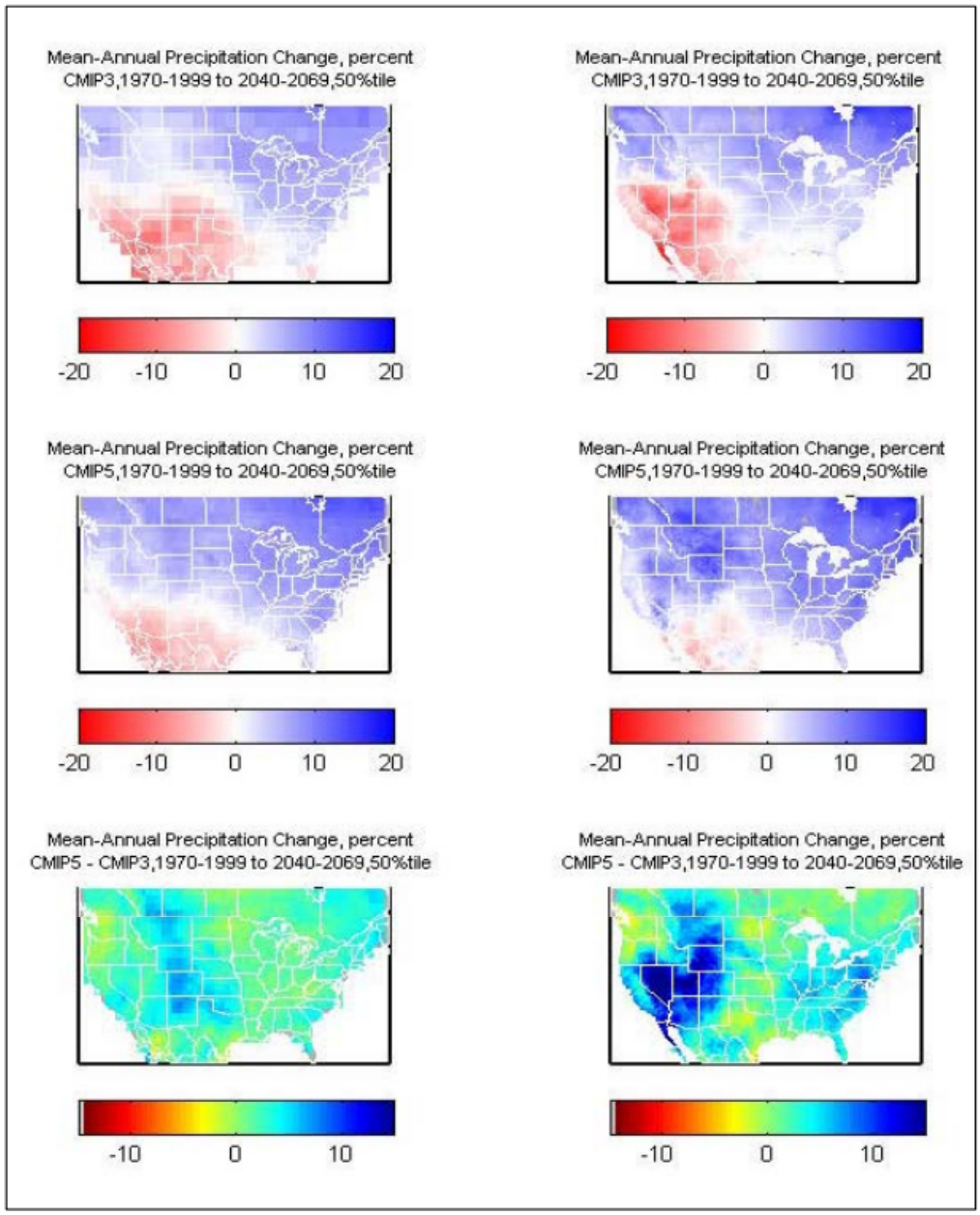

Figure 2.10 Change in mean annual precipitation over the contiguous United States from 1970–1999 to 2040–2069 for Bias-Correction/Spatial Disaggregation (BCSD) projections (Brekke et al., 2013)

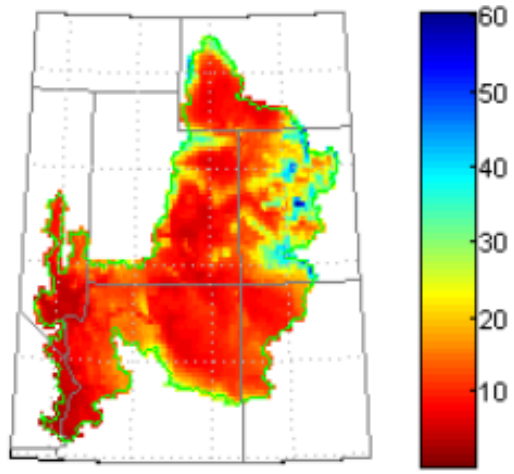

(a) Decade-mean precipitation of ensemble mean

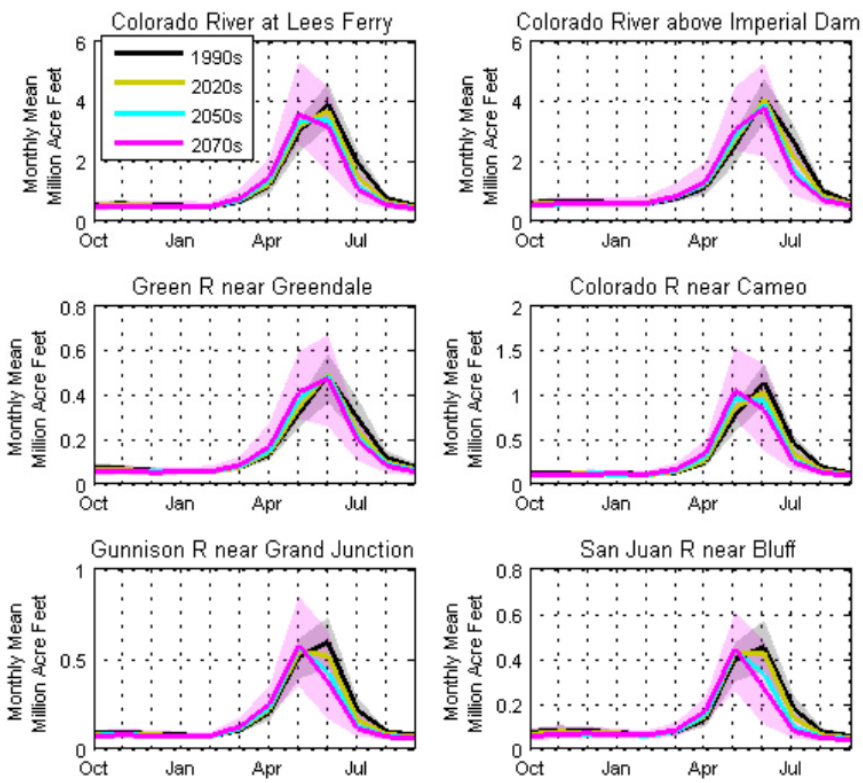

(b) Simulated mean-monthly runoff at various sub-basins

Figure 2.11 Climatologic and hydrologic projections for the Colorado basin

3. PHYSIOGRAPHIC AND CLIMATE DATA

Physiographical information is a crucial input in the IGISRM structure because it estimates parameters in a regression based on physiographic similarity to a target grid cell. High-resolution topographic data (~90 m pixels) generated by NASA's Shuttle Radar Topography Mission (SRTM) for the South Korea region were employed in this study. Topographic facets [Figure 3.1(c)] indicating contiguous terrain slope were extracted from the elevation data [Figure 3.1(b)] by identifying a direction with maximum slope among eight slopes calculated by distance and slope between a target grid and adjacent grid cells in the eight directions. Coastal proximity was designated on the basis of the elevation the target grid and the distance between the target grid and the ocean, as shown in Table 3.1. The corresponding values of coastal proximity from 1 to 6 at each grid were assigned according to the elevation and distance [Figure 3.1(d)].

Four statistical downscaling methods were developed and applied to South Korea, a country in the southern portion of the Korean Peninsula of 100,210 km^2 in area with complex topography including approximately 3,000 km^2 in islands. Because the spatial resolutions of GCMs are too coarse for describing the regional climate characteristics over South Korea, downscaling plays a crucial role in regional applications. Thus, an understanding of downscaling is an essential precursor for producing reliable downscaled climate scenarios from GCMs.

For historical validation, CFSR data set at 1.0° grid spacing over the period 1979 to the present (Saha et al., 2010) was selected. The latest CFSR is a coupled atmosphere, ocean, land, and sea ice reanalysis system with an interactive sea ice model, assimilation of satellite radiances for the entire period, and relatively high horizontal and vertical resolutions. Daily precipitation (PRCP), maximum temperature (TMAX) and minimum temperature (TMIN) of CFSR at 1.0° resolution were downscaled by the four statistical downscaling methods to the observational station network.

Table 3.1 Indexing coastal proximity corresponding to the elevation and horizontal distance from the coastline

Coastal proximity	Elevation (z)	Distance from the coastline (d)
1	$z \leq 200$ m	$d \leq 10$ km
2	$z > 200$ m	$d \leq 10$ km
3	$z \leq 200$ m	$10 < d \leq 20$ km
4	$z > 200$ m	$10 < d + \leq 20$ km
5	$z \leq 200$ m	$d > 20$ km
6	$z > 200$ m	$d > 20$ km

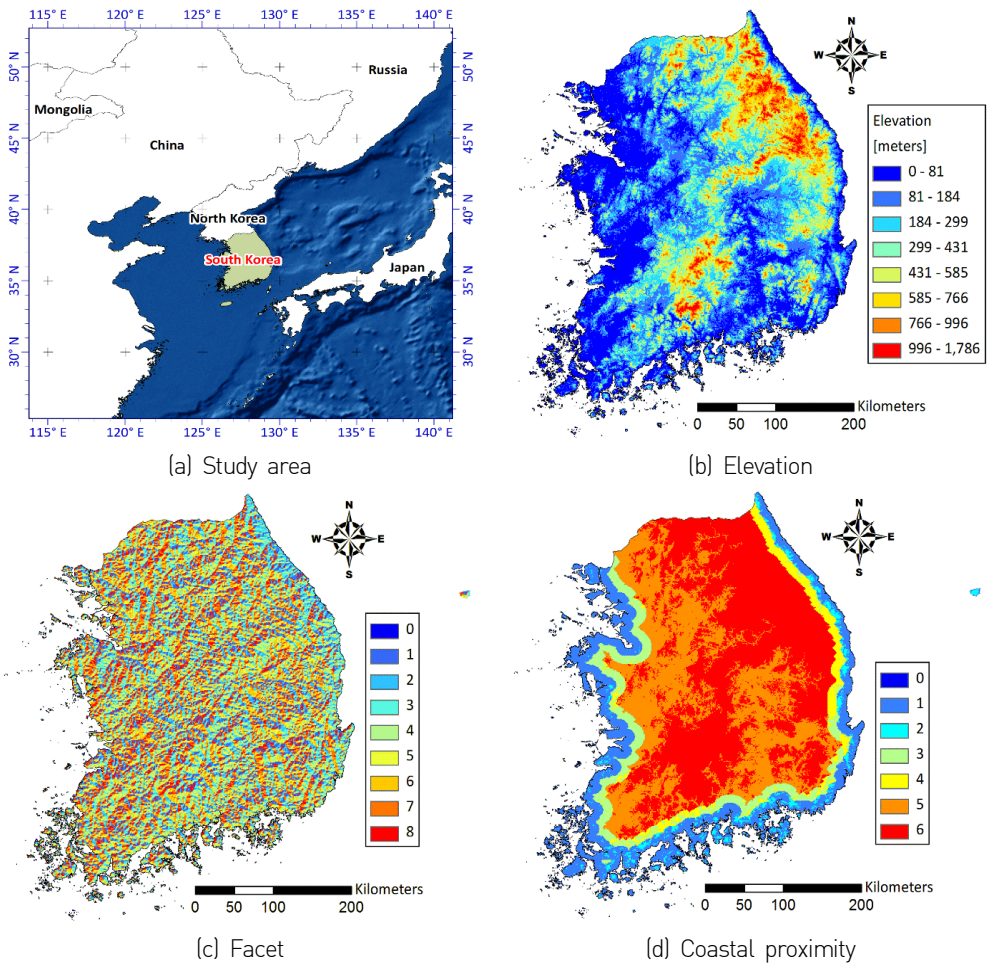

(a) Study area (b) Elevation

(c) Facet (d) Coastal proximity

Figure 3.1 Graphical maps of (a) study area, (b) elevation, (c) topographic facet, and (d) coastal proximity over South Korea

In South Korea, the Automatic Weather Station (AWS) and the Automated Synoptic Observing System (ASOS) networks provide observational climate data with inter-station spacing of approximately 12 km resolution [Figure 3.2(b)]. ASOS provides long-term climate data information of more than 30 years, whereas AWSs have been installed since 2000, thereby providing a short term datasets for only ~10–15 years. In general, a reliable long-term observed dataset is a prerequisite for applying statistical downscaling models that reflect the climate variability of a historical period. In this study, 60 stations [Figure 3.2(a)] were selected, which provide 9 observational climate variables PRCP, TMAX, TMIN, average air temperature, dew point temperature, average and maximum wind speed, and average and minimum humidity with few missing values for a common period of observational data from 1973 to 2010. Although the selected ASOSs are used to generate gridded datasets, the AWSs were employed in this study to validate the suggested IGISRM. That is, ASOSs were used to calibrate and generate a long-term gridded data from 1973 to 2010, and validation was implemented by comparing the generated data with observational data from 236 AWSs selected. For validation of the statistical downscaling methods, leave-one-out cross-validation with 38 years may provide overly optimistic estimates of skill owing to year-to-year persistence related to low-frequency climate variability such as El Niño Southern Oscillation (ENSO). However, leave-one-out cross-validation with 38 years can avoid the drawback of having a short data record for model validation. Therefore, we incorporated a split-sample validation approach with the first 19 years for calibration and the latest 19 years for validation.

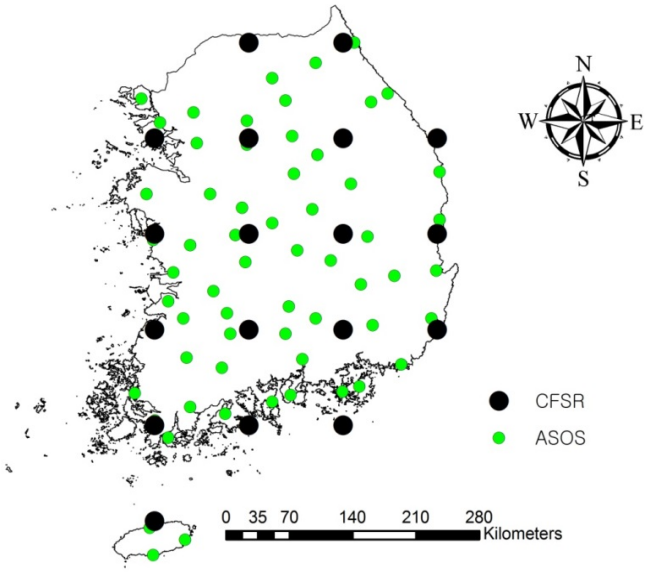

(a) ASOS and CFSR networks

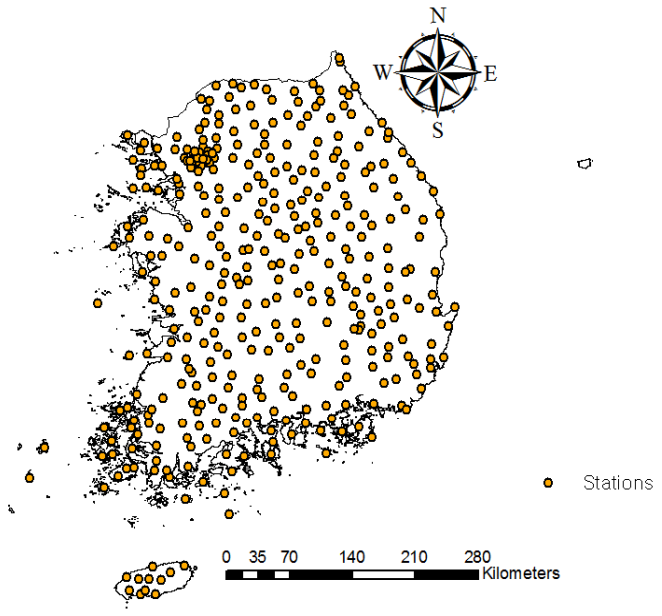

(b) AWS network

Figure 3.2 (a) Automated Synoptic Observing System (ASOS; green dots), Climate Forecast System Reanalysis (CFSR; black dots), and (b) Automatic Weather Station (AWS) surface networks over South Korea

4. METHDOLOGY

4.1 IGISRM

IGISRM introduces an iterative station density algorithm into a KNU/RM structure to determine the radius of influence that varies with the density of stations at each target grid cell. It is assumed that spatial distribution of climatology can be captured mainly by elevation. That is, elevation is the most important independent variable in a regression function because precipitation tends to generally increase and temperature tends to decrease as altitude increases (Barry and Chorley, 1987). Moreover, IGISRM incorporates the effects of terrain-induced climate transitions (facets) and coastal moisture sources into the regression function to determine station weighting in the algorithm.

IGISRM takes the form of a simple linear regression as in Eq. (1) because vertical distributions of climate are often linear (Hanson et al., 1982; Osborn, 1984). Moreover, it is used for simplicity and applicability in estimating climate variables compared with multiple regression schemes that have a complex relationship between multiple independent variables and climate.

$$\hat{y} = \beta_0 \hat{z} + \beta_1, \tag{1}$$

where $\hat{y}$ is the predicted climate variable; $\hat{z}$ is the elevation from SRTM at a target grid cell; and β_0 and β_1 are slope and intercept, respectively. The slope and intercept are determined by Eqs. (2) and (3).

$$\beta_0 = \sum_{i=1}^{n} w_i (y_i - \bar{y})(z_i - \bar{z}) \Big/ \sum_{i=1}^{n} w_i (z_i - \bar{z})^2 ; \;\; \beta_1 = \bar{y} - \beta_0 \bar{z} \tag{2}$$

$$\bar{y} = \sum_{i=1}^{n} w_i y_i \Big/ \sum_{i=1}^{n} w_i ; \;\; \bar{z} = \sum_{i=1}^{n} w_i z_i \Big/ \sum_{i=1}^{n} w_i \tag{3}$$

In Eq. (2) and Eq. (3), n is the number of stations within the radius of influence; w_i is the weighting of the ith station; and y_i and z_i are climate variable and elevation at the ith station, respectively. Therefore, the predictand is determined by elevation

and the predictor at stations located within a radius of the influence circle. In the KNU/RM, an initial radius of influence is applied to all grid cells in a domain and is expanded until the number of stations within the radius of influence over all grid cells reaches a minimum number of stations specified by the user (Lee et al., 2014). However, IGISRM calculates the radius of influence at each grid cell corresponding to the density of stations, as will be discussed in the following section. At a certain grid cell, the local climate–elevation relationship is not properly captured by sparse density of stations or a narrow range of elevation within the radius of influence. Such cases might arise mainly from a short radius or the lack of observational stations available in a domain. In particular, this study employed only 60 stations in South Korea, although the minimum number of stations in the radius is typically 10–30 (Daly et al., 2002). IGISRM increases the radius of influence until the minimum number of stations in the radius is set to three. Due to the limited number of stations within an influence radius, an unacceptable slope can be obtained when sparse observational stations exist near a target grid cell. On the basis of the historical record over South Korea, Hong et al. (2007) and Shin et al. (2008) calculated monthly maximum and minimum slopes, which are employed in IGISRM as a constraint in Eq. (1).

4.2 Combined weighting of station and iterative station density algorithm

The station weighting is obtained by a combination of weighting of distance, elevation, facet, and coastal proximity, as shown in Eq. (4):

$$w_i = (F_r w_r^2 + F_z w_z^2)^{0.5} w_f w_c, \tag{4}$$

where w_i is the combined weighting at the ith station; w_r, w_z, w_f and w_c are weights of distance, elevation, topographic facet, and coastal proximity, respectively; F_r and F_z are the importance factors for distance and elevation, respectively, that represent the relative importance between horizontal and vertical distances. Because the horizontal distance typically has a stronger influence on climate prediction modeling rather than on vertical distance, F_r and F_z were set to 0.8 and 0.2 in this study, as suggested in Daly et al. (2002).

The general form of the truncated Gaussian filter to calculate distance weighting at the center of a grid cell (p) is shown in Eq. (5) (Thornton et al., 1994):

$$w_r = \begin{cases} 0, & r > R_p \\ \exp\left[-\left(\frac{r}{R_p}\right)^2 \alpha\right] - e^{-\alpha}, & r \le R_p \end{cases}, \quad (5)$$

where w_r is the distance weighting with radial distance r from point p, R_p is the radius of the influence circle at a point p, and α is a non-dimensional shape parameter; this study employed the value of 6.25, as suggested in Thornton et al. (1994). The KNU/RM used a fixed radius of influence that guarantees a specified minimum number of stations, and weighting is obtained by the inverse distance method. However, a constant R_p may induce a large disparity of station numbers at regions with sparse or dense of stations. That is, a data-poor region has the least number of stations with non-zero weighting and vice versa. We suggest a modified iterative station density algorithm whereby R_p can be increased for a data-poor region and decreased for a data-rich region (Thornton et al., 1994). R_p is a function of the local station density for achieving regular station density specified by users over a domain. The procedure of modified iterative station density algorithm to obtain R_p is as follows:

1. An initial R_p is set over a domain. The radius derived from KNU/RM, 150 km, can be used as the initial value of R_p.

2. The local station density, D_p, is determined by Eq. (6), whereas w_i is obtained from Eq. (5), and $\overline{w}$ is the average weight defined by Eq. (7).

$$D_p = \frac{1}{\pi R_p^2} \sum_{i=1}^{n} \frac{w_i}{\overline{w}} \quad (6)$$

$$\overline{w} = \frac{1}{\pi R_p^2} \int_0^{R_0} w_r \, dr = \left(\frac{1 - e^{-\alpha}}{\alpha}\right) - e^{-\alpha} \quad (7)$$

3. By using the local station density, a new R_p value is obtained with the average number of stations, N, by Eq. (8). In this study, the average number of stations was set to 5.

$$R_p = \sqrt{\frac{N}{\pi D_p}} \tag{8}$$

2. Substituting R_p calculated by Eq. (8) into Eq. (6), steps (2) and (3) are iterated until the stop conditions are satisfied. Thornton et al. (1994) used a stop condition such that the maximum number of iterations is reached. The present study introduces two stop conditions. The first is a tolerance (= 0.0001) for the absolute difference value of R_p between the previous and current iterations, and the second is the maximum number of iteration in this study (50).

As a pre-process, once R_p at each grid cell is specified, the value is used over a time horizon to calculate station weighting.

Elevation weighting, w_z, represents the influence of stations by the altitudinal range of climate data. That is, the elevation weighting expressed by Eq. (9) decreases with the vertical distance between a target grid cell and a station:

$$w_z = \begin{cases} \frac{1}{\Delta z_{min}}, & if\ \Delta z \le z_{min} \\ \frac{1}{\Delta z}, & if\ z_{min} < \Delta z < z_{max} \\ 0, & if\ \Delta z \ge z_{max} \end{cases} \tag{9}$$

where Δz represents the vertical distance from a target cell to a station, and Δz_{min} and Δz_{max} are the minimum and maximum vertical distances, which were set to 100 m and 500 m in this study, respectively.

In addition, the weights of topographic facet and coastal proximity, w_f and w_c, are calculated by Eq. (10) and Eq. (11), respectively:

$$w_f = \begin{cases} 1, & if\ f \le 1 \\ \frac{1}{\Delta f}, & if\ f > 1 \end{cases} \tag{10}$$

$$w_c = \begin{cases} 1, & if\ c = 0 \\ \frac{1}{\Delta c}, & if\ 0 < c < c_{max} \\ 0, & if\ c \ge c_{max} \end{cases} \tag{11}$$

where Δf is absolute orientation difference between a target cell and a station

within R_p. When $f = 1$, the orientation difference is either the same or 180°. Δc is the difference in coastal proximity between a target cell and a station. The coastal proximity has been indexed from 1 to 6 corresponding to the distance between a coastline and elevation, as shown in Table 1.

4.3 Precipitation and temperature predictions

Precipitation predictions have a complex system that needs to predict both the precipitation occurrence and the total amount of precipitation. Given the assumption that the patterns of precipitation occurrence are spatially coherent at the daily time scale, precipitation occurrence is defined by a function of weighted precipitation occurrence at the stations within the radius of influence, as shown in Eq. (12):

$$\mathrm{POP} = \sum_{i=1}^{n} w_i PO_i \Big/ \sum_{i=1}^{n} w_i , \qquad \mathrm{PO}_i = \begin{cases} 0, & if \;\; P_i = 0 \\ 1, & if \;\; P_i > 0 \end{cases}, \tag{12}$$

where POP represents the probability of precipitation occurrence, and PO_i is a binomial variable that becomes 0 when the amount of precipitation at the ith station is 0 and 1 when the amount of precipitation at the ith station is above 0. With such a simple binomial predictor, this study defines the precipitation occurrence as that when the POP is above 0.5.

The prediction methods for minimum and maximum air temperature are identical to the procedure for precipitation except they incorporate POP. That is, the same linear equation for the expressed and combined weighting in Eq. (1) and Eq. (4) is used with the same radius of influence, R_p, to estimate the minimum and maximum temperature in this study.

4.4 Statistical downscaling methods

4.4.1 Simple Spatial Interpolation

As the simplest downscaling method, Simple Spatial Interpolation (SDI) is conducted to produce downscaled values at each station by using the inverse distance technique (Lapen and Hayhoe, 2003). Therefore, downscaled values preserve the bias of the climate model, which varies with the level of topographical complexity at each station. This means that the skill of SSI is dependent entirely on the skill of the climate model. Therefore, SSI can be a standard for the skill of the climate model, and the effects of statistical downscaling methods can be quantitatively evaluated by measuring the improvement in the downscaling skill.

4.4.2 Bias-Correction/Spatial Disaggregation

BCSD was originally developed to downscale GCM output to provide input data for macro-scale process-based hydrologic models (Wood et al., 2004). Traditionally, BCSD downscales at a monthly time step and temporally disaggregates to a daily time step by randomly selecting daily sequences from the historical dataset (Maurer and Hildago, 2008; Werner et al., 2013). The use of BCSD has been extended for direct downscaling at the daily scale (Abatzoglou and Brown, 2012; Thrasher et al., 2012), which is employed for the inter-comparison of statistical downscaling methods in this study. Because daily BCSD performs spatial disaggregation and bias-correction with daily coarse-resolution climate data, this method does not require temporal disaggregation. As a result, it maintains the daily spatial and temporal structure of the coarse-resolution data. Therefore, the skill of the coarse-resolution data plays an important role in the performance of daily BCSD.

Daily BCSD first spatially disaggregates coarse-resolution data to a finer resolution by an inverse distance interpolation scheme (Lapen and Hayhoe, 2003). It then applies bias correction by using a quantile mapping algorithm that equates the empirical cumulative distribution functions (CDFs) of observed and modeled data, F_o and F_m, respectively:

$$\hat{x}_m(t) = F_o^{-1}[F_m\{x_m(t)\}] \quad (13)$$

where $\hat{x}_m(t)$ and $x_m(t)$ are bias-corrected and modeled data at time t, respectively. Although the majority of the model outputs can be corrected by Eq. (13), some extreme cases may be out of the range of the historical data. For such cases, the CDFs are estimated by parametric distribution functions, and the corresponding values are then extrapolated. For precipitation, Weibull and Gumbel distributions are employed for low and high events, respectively, whereas a normal distribution is employed for temperature. To formulate the sample CDFs, we used observational and modeled daily data within 15-day moving windows centered on each calendar day.

4.4.3 Bias Correction/Constructed Analog

A primary assumption of analog downscaling methods is that a weather pattern in the historical record should be replicated in the future (Lorenz, 1969; van den Dool, 1994). By incorporating a relationship of coarse- and fine-scale historical data, the current weather patterns, and a specified GCM weather event, useful coarse-scale analogs can be constructed for downscaling (Timbal et al., 2003; van den Dool, 2003; Diez et al., 2005). Because a linear combination of multiple patterns rather than a single analog (Fernández and Sáenz, 2003) provides added-values in forecasts (van den Dool, 2003), a best-fit analog is constructed by a linear combination of multiple coarse-resolution historical weather patterns, known as a library, that matches the bias-corrected GCM weather pattern on a given date. The fine-resolution historical data are aggregated to the resolution of the climate model to form the library. Then, the constructed analog weights at coarse resolution are applied to the fine-resolution weather patterns on same dates to produce downscaled outputs. Maurer and Hildago (2008) reported that the greatest skill is obtained by using precipitation and temperature as predictors; thus, the library is composed of precipitation and temperature patterns in the present study. Bias correction was applied to the coarse-resolution GCM data by using quantile mapping. Hence, following Maurer et al. (2010), absolute values were used to identify analogs in BCCA rather than anomalies.

Mathematically, the target pattern ($\mathbf{T}_m$) should be defined, as shown in Eq. (14), by the regression coefficient matrix ($\mathbf{A}_{\text{analog}}$) and analog patterns ($\mathbf{C}_{\text{analog}}$) composed of the best 10 days. These days are selected on the basis of root–mean–square error (RMSE) between the target pattern and the historical weather patterns in the library during the calibration period.

$$\mathbf{T}_m = \mathbf{C}_{\text{analog}}\ \mathbf{A}_{\text{analog}} \tag{14}$$

Applying the Moore–Penrose inverse to $\mathbf{C}_{\text{analog}}$, $\mathbf{A}_{\text{analog}}$ can be obtained by Eq. (15).

$$\mathbf{A}_{\text{analog}} = \left[\left(\mathbf{C}'_{\text{analog}}\,\mathbf{C}_{\text{analog}}\right)^{-1}\mathbf{C}'_{\text{analog}}\right]\mathbf{T}_m \tag{15}$$

For precipitation, the matrix to be inverted in Eq. (15) is often a near-singular matrix, for example, when the domain is dominated by dry grid cells. Therefore, this study employed the ridge regression technique (Tikhonov et al., 1995) with a small penalty to solve in these cases. The same regression coefficient matrix ($\mathbf{A}_{\text{analog}}$) ws applied to the fine-resolution weather patterns on the same days that correspond to the date of the constructed analog ($\mathbf{C}_{\text{analog}}$) at coarse resolution. That is, the downscaled values ($\mathbf{V}_{\text{downscaled}}$) are obtained by Eq. (16):

$$\mathbf{V}_{\text{downscaled}} = \mathbf{V}_{\text{analog}}\left[\left(\mathbf{C}'_{\text{analog}}\right)^{-1}\mathbf{C}'_{\text{analog}}\right]\mathbf{T}_m, \tag{16}$$

where $\mathbf{V}_{\text{analog}}$ is a constructed fine-resolution analog, i.e., the spatial pattern of climate variables over the 60 stations.

4.4.4 Multivariate Adapted Constructed Analogs

Mathematically, MACA follows the same procedure as BCCA except that it incorporates additional variables into the analogs at both coarse and fine resolutions. An epoch adjustment that removes and re-introduces the differences in mean values between the current and future time slices (e.g., 1990s and 2050s) in the original MACA methodology (Abatzoglou and Brown, 2012) was skipped in this study because this study downscaled the CFSR dataset over a relatively stationary historical period. After analyzing the correlations between variables (Table 4.1), MACA was conducted

jointly for PRCP with minimum humidity and for TMAX and TMIN with average temperature to improve the coherence in spatial weather patterns on a given day. Thus, this study can evaluate the added-value of MACA, which introduces additional variables into the constructed analogs relative to BCCA.

4.4.5 Bias-Correction/Climate Imprint

A spatial climate imprint that represents climate gradients at both coarse and fine resolutions was obtained from the mean value at each grid point for the calibration period of 1973–1991. Similar to that in BCCA and MACA, the fine-resolution historical data are aggregated to the CFSR spatial resolution prior to bias correction by quantile mapping. The ratios of daily model output relative to the mean values at the coarse resolution were calculated for PRCP and were then spatially interpolated to the fine (station-based) resolution. The interpolated ratios were multiplied by the mean values at each station to obtain the downscaled values [Eq. (17)]. For TMAX and TMIN, the differences between the daily model output and the long-term mean values were used instead of the ratios [Eq. (18)]:

$$P_{\text{downscaled}}(t) = R_{\text{interpolated}}\, P_{\text{ave}}, \tag{17}$$

$$T_{\text{downscaled}}(t) = T_{\text{ave}} - D_{\text{interpolated}}, \tag{18}$$

where $P_{downscaled}$ is the downscaled PRCP, $R_{interpolated}$ is the spatially interpolated ratio at each station, P_{ave} is the long-term mean precipitation at each station, $T_{downscaled}$ is the downscaled TMAX or TMIN, $D_{interpolated}$ is the spatially interpolated difference for each station, and T_{ave} is the long-term mean temperature at each station.

Table 4.1 Averaged correlation coefficients of climate variables at Automated Synoptic Observing System (ASOS) sites. Bold values represent the maximum correlation between the variables.

Variables	PRCP	Tave	TMAX	TMIN	Tdew	Wave	Wmax	Have	Hmin
PRCP	1.00	0.17	0.10	0.22	0.24	0.06	0.10	0.33	**0.39**
Tave		1.00	**0.98**	**0.98**	0.96	−0.16	−0.17	0.37	0.36
TMAX			1.00	0.92	0.91	−0.22	−0.20	0.30	0.22
TMIN				1.00	0.97	−0.13	−0.16	0.45	0.47
Tdew					1.00	−0.22	−0.22	0.61	0.56
Wave						1.00	0.82	−0.30	−0.10
Wmax							1.00	−0.25	−0.13
Have								1.00	0.84
Hmin									1.00

Tave: average temperature; Tdew: dew point temperature; Wave: average wind speed; Wmax: maximum wind speed; Have: average humidity; Hmin: minimum humidity

Table 4.2 Contingency table for categorizing a binary event of prediction. The sum of all events is the number of observations: N = a + b + c + d

Prediction	Observed		
	Yes	No	Total
Yes	a	b	a + b
No	c	d	c + d
Total	a + c	b + d	N = a + b + c + d

4.5 Performance measures

4.5.1 Assessment of regression model skill

Water resources management in South Korea is generally planned per each city or county, which requires a spatial resolution of at least 5 km. By using 60 ASOSs over South Korea, therefore, we generated long-term gridded datasets with IGISRM at various levels of spatial resolution from 1 km to 5 km to select an ideal resolution based on both performance measures and computational efficiency. The assessment of model performance was conducted by correlation coefficient (CC), bias, mean absolute error (MAE), and RMSE, as shown in Eq. (19) to Eq. (22).

$$CC = \frac{\sum(P_i - \bar{P})\,(O_i - \bar{O})}{\sqrt{\sum(P_i - \bar{P})^2}\sqrt{\sum(O_i - \bar{O})^2}}, \tag{19}$$

$$Bias = \frac{\sum(P_i - O_i)}{\sum O_i}, \tag{20}$$

$$MAE = \frac{1}{N}\sum|P_i - O_i|, \tag{21}$$

$$RMSE = \sqrt{\frac{\sum(P_i - O_i)^2}{N}}, \tag{22}$$

where P_i and O_i are predicted and observed values, respectively, and N is the total number of time horizons at the stations.

Because KNU/RM uses a fixed radius of influence circle at all grid cells, a longer radius can be obtained at a poor-density region to guarantee the minimum number of stations within the radius. The spatial continuity of precipitation is much less than that of other variables such as air temperature and humidity, particularly in a complex topographic region. In the case with a longer radius of influence, therefore, many wet days with negligible amounts of precipitation can occur in many grid cells; this phenomenon is known as the drizzling effect. That is, KNU/RM may generate too many wet days in a year compared with observational station data. Therefore, we evaluated five performance measures that focus on the correspondence of

precipitation occurrence between predictions and observations (Murphy, 1997): frequency bias of occurrence (FBias; Donaldson et al., 1975), hit rate (H; Swets, 1986), false-alarm ratio (FAR; Donaldson et al., 1975), proportion correct (PC; Finley, 1884), and critical success index (CSI; Gilbert, 1884). The definitions of the five performance measures are described in Eq. (23) to Eq. (27), respectively, which are functions of the number of successes and failures of prediction based on the four possible combinations of predictions and observations as shown in the contingency table (Table 4.2).

$$FBias = \frac{a+b}{a+c} \tag{23}$$

$$H = \frac{a}{a+c} \tag{24}$$

$$FAR = \frac{b}{a+b} \tag{25}$$

$$PC = \frac{a+d}{a+b+c+d} \tag{26}$$

$$CSI = \frac{a}{a+b+c} \tag{27}$$

FBias represents the ratio of the number of predictions of occurrence to the number of observed occurrences. A perfect score of *FBias* is equal to 1; that above 1 represents a higher number of wet days from predictions than that from the observations. On the contrary, a value of less than 1 of indicates a lower number of wet days in the predictions. *H* represents the ratio of correct predictions for precipitation occurrences, which is also termed as probability of detection (Donaldson et al., 1975). Sometimes *H* is termed to represent *PC* (Wilks, 1995). However, this study distinguishes the two measures to identify the effectiveness of IGISRM in predicting rainy or no-rainy days at all grid cells. *FAR* is an estimate of conditional probability of a false alarm given that rainy days are predicted; 0 represents a perfect ratio. *CSI* represents an estimate of the conditional probability of a hit given that the rainy days are predicted, observed, or both; a perfect score is 1.

Therefore, this study estimates both quantitative and qualitative performance measures for precipitation that has relatively large spatial heterogeneity, whereas only quantitative performance measures for TMIN and TMAX are used for inter-comparison between IGISRM and PRISM.

Severe socio-economic impacts on natural and infrastructural systems are induced by extreme events such as floods, drought, and heat and cold waves (Butt et al., 2011; Wernberg et al., 2012). The requirements for analyzing the impacts related to extreme climate events have been increasing at regional and global scales (Tebaldi et al., 2006; Kharin et al., 2007; Min et al., 2011; Zhang et al., 2005; Burgers et al., 2012). The ability of IGISRM and KNU/RM for reproducing extreme climate indices in reference to ETCCDI (www.climdex.org; Zhang et al., 2011; Sillmann et al., 2013) was evaluated in this study. All ETCCDI indices were calculated annually, and the numbers of heavy precipitation (Rnnmm), equal to or greater than different thresholds were increased by 10 mm from 10 mm to 80 mm to investigate the changes in the performances of IGISRM and KNU/RM corresponding to different levels of heavy rainfall. By using 236 AWS datasets from 2000 to 2010, we inter-compared the skill of the two GIS-based regression models, IGISRM and KNU/RM, to reproduce extreme events by using the correlation coefficient and the K–S D statistic (Murdock et al., 2013), which represents the supremum (maximum) distances of the empirical distributions between observations and generated data.

4.5.2 Assessment of downscaling skill

The downscaled daily PRCP, TMAX, and TMIN from CFSR for the validation period from 1992 to 2010 were assessed by using four performance metrics. The first metric measures the ability to reproduce the temporal sequencing of events, i.e., the correlation between the observation and downscaled values. The spatial and temporal structure of the daily climate model is preserved in the daily downscaling methods used in this study. Therefore, the daily skill on this metric is highly dependent on the skill of the climate model. However, improvement in downscaling skill can be assessed by comparing results from Simple Spatial Interpolation (SSI). The second metric measures the ability to reproduce the distribution of observed values estimated

by the K-S D statistic. The third metric measures the ability to reproduce observed spatial patterns, which is measured by the RMSE of the spatial correlations between observed and downscaled datasets. The fourth metric is based on the 23 ETCCDI indices listed in Table 4.3, which have been recommended by the World Meteorological Organization to detect changes in precipitation- and temperature-related extremes (Zhang et al., 2011). Skill is given by the average proportion of stations passing two-sample K–S tests at the 5% significance level for each of the 23 ETCCDI indices. To evaluate the skill for each variable (PRCP, TMAX, and TMIN), we separated the 23 indices into three categories, as indicated in the second column in Table 2. For example, we considered the proportion of passed K–S tests on SU, ID, TXx, TXn, TX10, TX0, SWDI, and DTR indices to evaluate the skill for TMAX. To summarize, the performance metrics evaluate downscaling skill in terms of 1) daily sequence, 2) distribution, 3) spatial correlation, and 4) extremes.

Table 4.3 Expert Team on Climate Change Detection and Indices (ETCCDI) indices employed in this study

ID	Variable	Description	Unit
SU	TMAX	Annual count of days when TMAX > 25°C	Days
ID		Annual count of days when TMAX < 0°C	Days
TX_n		Annual minimum value of TMAX	°C
TX_x		Annual maximum value of TMAX	°C
TX10p		Percentage of days when TMAX < 10^{th} percentile	%
TX90p		Percentage of days when TMAX > 90^{th} percentile	%
WSDI		Annual count of days with at least 6 consecutive days when TMAX > 90^{th} percentile	Days
FD	TMIN	Annual count of days when TMIN < 0°C	Days
TR		Annual count of days when TMIN > 20°C	Days
TN_n		Annual minimum value of TMIN	°C
TN_x		Annual maximum value of TMIN	°C
TN10p		Percentage of days when TMIN < 10^{th} percentile	%
TN90p		Percentage of days when TMIN > 90^{th} percentile	%
CSDI		Annual count of days with at least 6 consecutive days when TMIN < 10^{th} percentile	Days
DTR	TMAX & TMIN	Annual mean difference between TMAX and TMIN	°C
CDD	PRCP	Maximum number of consecutive days with daily PRCP < 1 mm	Days
CWD		Maximum number of consecutive days with daily PRCP ≥ 1 mm	Days
PRCPTOT		Annual total PRCP in wet days (daily PRCP ≥ 1mm)	mm
Rx1day		Annual maximum one-day precipitation	mm
Rx5day		Annual maximum five-day precipitation (PRCP)	mm
R95pTOT		Annual total PRCP when daily PRCP > 95 percentile	mm
R99pTOT		Annual total PRCP when daily PRCP > 99 percentile	mm
SDII		Annual precipitation divided by the number of wet days	mm/day

4.6 Technique for Order of Preference by Similarity to Ideal Solution

A goal of this study is to identify a robust technique from the four statistical downscaling methods considered in this study for South Korea. The use of multiple performance criteria means that models may perform well in some areas but not others, which can lead to ambiguity when making a final recommendation. Therefore, we introduce the use of TOPSIS, a systematic process for determining suitable alternatives to a multi-criteria problem. The only assumption of TOPSIS is that all utility functions should be monotonically increasing or decreasing. Because of its simplicity, TOPSIS has been applied to a range of problems including business model comparison (Zhou et al., 2012), assessment of the sea value of coastal areas (Wang and Peng, 2015), transportation systems (Awasthi et al., 2011), and watershed management (Chung and Lee, 2009; Jun et al., 2013; Lee et al., 2013). TOPSIS begins by creating an evaluation matrix, $(x_{ij})_{m \times n}$, for the ith alternative and jth criterion. Then, the weighted normalized decision matrix, $(t_{ij})_{m \times n}$, is given by

$$\left(t_{ij}\right)_{m \times n} = \left(w_j n_{ij}\right)_{m \times n} \quad i = 1,2,\cdots,m; \;\; j = 1,2,\cdots,n; \tag{28}$$

$$n_{ij} = \frac{x_{ij}}{\sum_{i=1}^{m} x_{ij}^2}, \tag{29}$$

where n_{ij} is the normalized matrix from x_{ij} by the vector normalization [Eq. (29)], and w_j represents weighting on the jth criterion (Hwang and Yoon, 1981). We used equal weighting (= $1/n$) for simplicity. Then, determination of the worst (A_w) and best (A_b) conditions [Eq. (30) and (31)] is necessary to calculate Euclidean distances from the worst and best conditions at the target alternatives, d_{iw} and d_{ib}, using Eq. (32) and Eq. (33), respectively.

$$A_w = \left\{\left\langle \max\left(t_{ij} \,|\, i = 1,2,\cdots,m\right) | \, j \in J_- \right\rangle, \left\langle \min\left(t_{ij} \,|\, i = 1,2,\cdots,m\right) | \, j \in J_+ \right\rangle\right\} \equiv \left\{t_{wj} \,|\, j = 1,2,\cdots,n\right\} \tag{30}$$

$$A_b = \left\{\left\langle \min\left(t_{ij} \,|\, i = 1,2,\cdots,m\right) | \, j \in J_- \right\rangle, \left\langle \max\left(t_{ij} \,|\, i = 1,2,\cdots,m\right) | \, j \in J_+ \right\rangle\right\} \equiv \left\{t_{bj} \,|\, j = 1,2,\cdots,n\right\} \tag{31}$$

$$d_{iw} = \sqrt{\sum_{j=1}^{n}(t_{ij} - t_{wj})^2} \quad i = 1,2,\cdots,m \tag{32}$$

$$d_{ib} = \sqrt{\sum_{j=1}^{n}(t_{ij} - t_{bj})^2} \quad i = 1,2,\cdots,m \tag{33}$$

For the four performance metrics (n = 4) from the four downscaling methods (m = 4) in this study, for example, $(x_{ij})_{4 \times 4}$ was evaluated, and the weighted and normalized matrix (t_{ij}) was be obtained. The worst and best conditions (A_w and A_b) are determined according to the rescaled metrics (t_{ij}) and characteristics of each performance metric including the first and fourth metrics (i.e., the correlation and the average proportion of stations passing K–S tests) are in J_+, and the second and third metrics (i.e., the K–S D statistic and RMSE of spatial correlation) are in J_-. For example, t_{w1} and t_{b1} are the minimum and maximum values of correlations from the four downscaling methods, respectively. By using Eq. (32) and Eq. (33), the Euclidean distances from the worst condition and best condition for each downscaling method were calculated.

As a final step in TOPSIS, we ranked all alternatives based on the similarity [Eq. (34)] for determining suitable alternatives or excluding worst alternatives by introducing a cut-off threshold.

$$s_{iw} = \frac{d_{iw}}{d_{iw} + d_{ib}}, 0 \le s_{iw} \le 1, \quad i = 1,2,\cdots,m \tag{34}$$

When s_{iw} = 1, the alternative is equal to the best condition; s_{iw} = 0 indicates that the alternative is equal to the worst condition. That is, the ith statistical downscaling method nearest to s_{iw} = 1 can be considered as the most suitable and robust method and vice versa.

5. RESULTS AND DISCUSSION

5.1 Decision of influence radius

In the IGISRM procedure, all grid cells in a domain have different radii of influence, R_p, depending on the station density within the R_p. Figure 5.1 shows the spatial distribution of R_p decided by the iterative station density algorithm. As shown in the figure, the R_p ranges from 41 km to 268 km, where station-adjacent regions represented by green dots in Figure 2.2, are shown in blue, and regions far from stations are represented by yellow or red colors. In particular, the northern and northeastern areas, which are data-poor regions, showed longer R_p than those at the other regions. Such results indicate that the R_p calculated by the modified iterative station density algorithm properly capture the spatial distribution of station density at each grid cell. We also determined the radius of influence circle to implement the KNU/RM as 150 km to include the minimum number of stations over all grid cells in South Korea. Although this study sets the target number of stations within R_p at five for IGISRM, the minimum number of stations is obtained as three at several grid cells near small islands owing to the maximum iteration constraint. KNU/RM provides the same minimum number of stations with the fixed influence radius of 150 km as that in IGISRM.

5.2 Assessment of IGISRM performance in selecting the spatial resolution of gridded data

Determination of spatial resolution is an important step before generating gridded data with IGISRM. Very high resolutions such as 0.5 km or 1 km require higher computational burdens and data storage capacities. However, it is generally difficult to capture the impacts of physiographical characteristics in climate variables when a coarse resolution is used deu to the smoothing effect by averaging the topographic features at each grid cell (Cherubini et al., 2002; Petrik et al., 2011). Therefore, we tested the various levels of spatial resolution to identify a threshold grid spacing that may show a sharp shift in the level of accuracy. Because water resource managers

in South Korea need at least 5 km resolution to build a long-term plan for each of city or county, we tested IGISRM with five different spatial resolutions from 1 km to 5 km to identify the most suitable resolution with regard to accuracy and computational efficiency.

The four performance measures—CC, RMSE, MAE, and Bias—corresponding to each spatial resolution are presented in Table 5.1. All numbers were averaged over all grid cells located in South Korea. Each gridded data set was generated for 38 years from 1973 to 2010, and the four measures were then evaluated by comparing AWS station data from 2000 to 2010 for validation. As expected, 1 km resolution provided the best performance on most measures for all variables including PRCP, TMAX, and TMIN. Interestingly, we found that 3 km is the critical threshold of spatial resolution that shows a sharp change in performance for TMAX and TMIN, although the performance for PRCP was similar at each resolution.

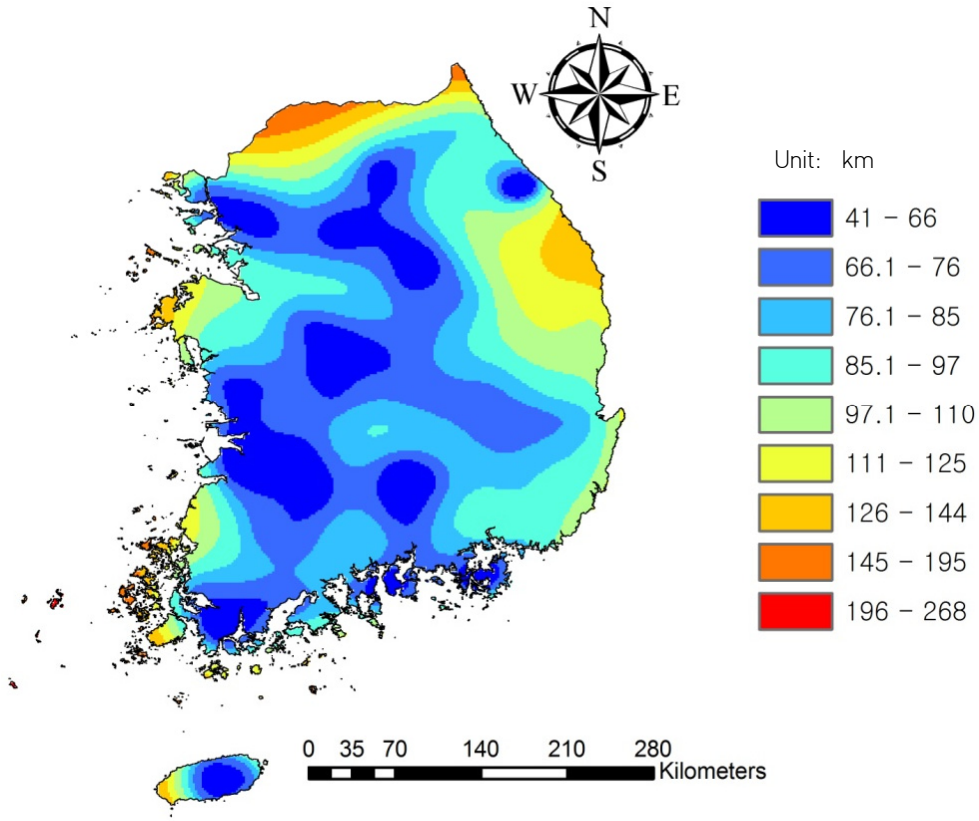

Figure 5.1 Spatial distribution of radius of influence (R_p) obtained by an iterative station density algorithm in the Improved GIS-based Regression Model (IGISRM)

Table 5.1 Evaluation of performance measures of the Improved GIS-based Regression Model (IGISRM) for precipiation and minimum and maximum air temperatures corresponding to the five spatial resolutions

Climate variable	Measure	Resolution/number of grid cells				
		1 km/ 391,476 (646 × 606)	2 km/ 98,496 (324 × 304)	3 km/ 44,268 (217 × 204)	4 km/ 25,256 (164 × 154)	5 km/ 16,368 (132 × 124)
Precipi-tation (PRCP)	CC	0.85	0.86	0.86	0.86	0.85
	RMSE	7.47	7.43	7.40	7.31	7.71
	MAE	1.83	1.84	1.84	1.85	1.92
	Bias	0.02	0.06	0.06	0.07	0.13
Maximum temperature (TMAX)	CC	0.99	0.99	0.99	0.99	0.99
	RMSE	1.54	1.55	1.58	1.77	1.91
	MAE	1.19	1.21	1.24	1.41	1.52
	Bias	−0.11	−0.17	−0.05	−0.23	−0.20
Minimum temperature (TMIN)	CC	0.98	0.98	0.98	0.98	0.98
	RMSE	2.28	2.48	2.39	2.52	2.74
	MAE	1.62	1.81	1.72	1.84	2.04
	Bias	0.08	−0.02	0.12	−0.17	0.28

To clearly identify the change point of spatial resolution in performance, all measures were normalized and summed to avoid the scale effect, where only CC took the reverse form. Figure 5.2 represents the summation scores for PRCP, TMAX, and TMIN corresponding to each spatial resolution, where a lower value indicates better performance. The scores of coarser resolutions, 4 km and 5 km, are visually higher than those of finer resolutions. Although the performance varied with each variable, the sums of scores at 1 km to 3 km for the three variables were 16.5, 16.7, and 16.6, respectively, showing strongly compatible performances. However, the difference in grid cell between 1 km and 3 km was 347,208 cells, and 1 km resolution also needs approximately 13-hour additional computational time to complete the generation of gridded data for 38 years compared with that at 3 km. Such results indicate that the most suitable spatial resolution of gridded data might be 3 km with regard similar accuracy and less computational time. Therefore, 3 km resolution was selected as the most suitable grid spacing.

5.3 Inter-comparison of IGISRM and KNU/RM

Inter-comparison of the performances between IGISRM and KNU/RM at 3 km resolution was implemented on the basis of the four performance measures [Eqs. (19) to (22)] used in the selection of spatial resolution and an additional five performance measures related to precipitation occurrence [Eqs. (23) to (27)].

Figure 5.3 shows the spatial distribution of the four measures for only PRCP, which typically shows higher spatial variability. Overall, the two schemes generated less accurate climate data in the eastern area, where sparse station networks exist owing to mountainous topography. In addition, the areas showing less skill by IGISRM, represented in the figure by light or red colors, are smaller than those by KNU/RM. Near the center of South Korea, where the station density is relatively higher, IGISRM produced better results for RMSE [Figure 5.3(b)], MAE [Figure 5.3(c)], and Bias [Figure 5.3(d)]. The performance measures of IGISRM and KNU/RM for PRCP, TMAX, and TMIN during each season and for the total period are presented in Figure 5.4.

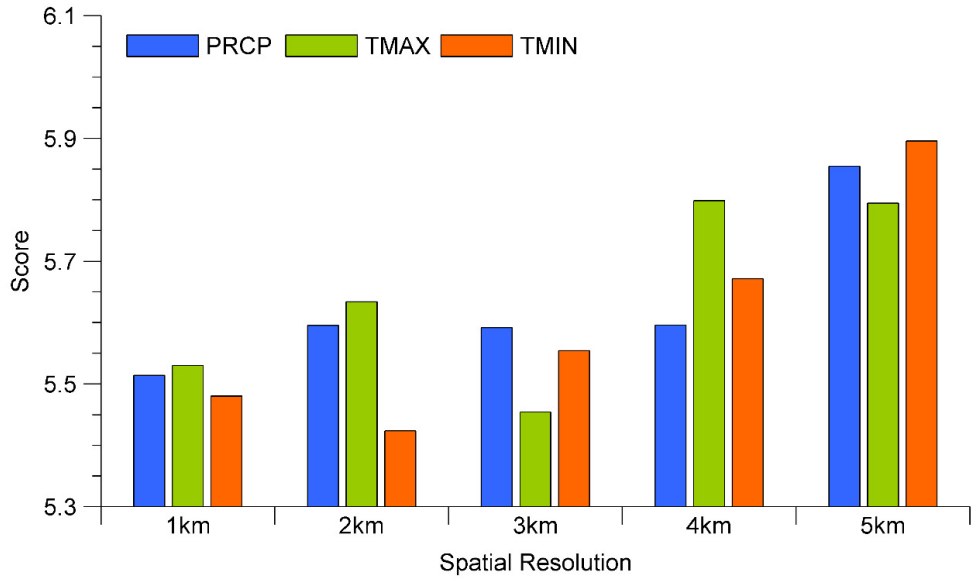

Figure 5.2 Summation of normalized measures for precipitation (PRCP), maximum temperature (TMAX), and minimum temperature (TMIN) corresponding to the five spatial resolutions tested in this study

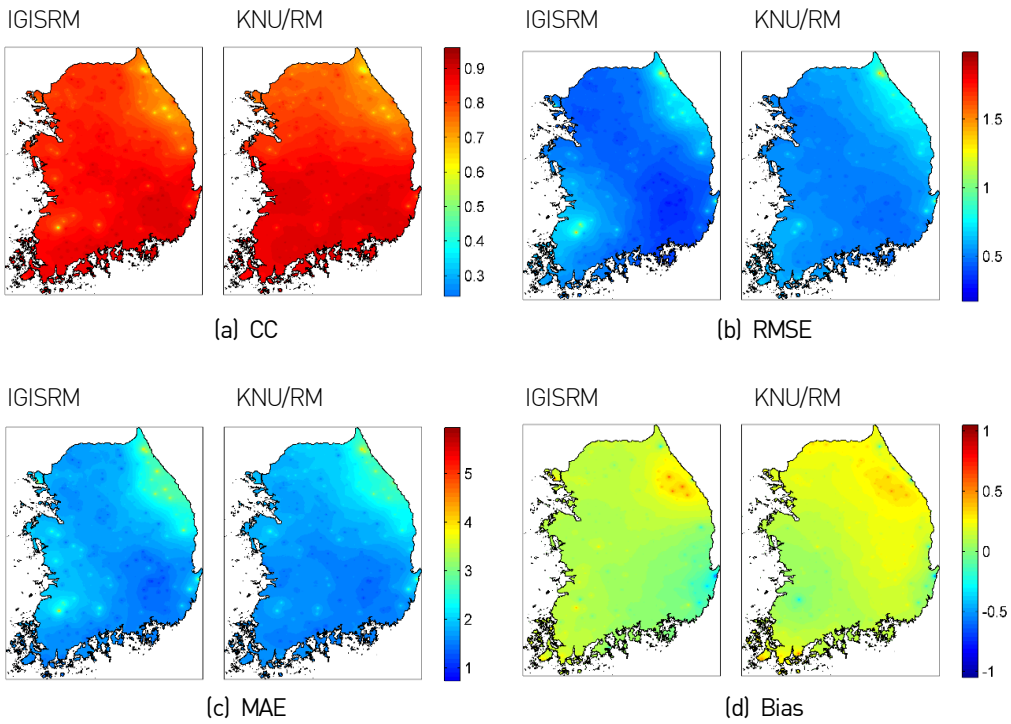

Figure 5.3 Spatial map of performance measures of the Improved GIS-based Regression Model (IGISRM) and the previous regression model of Kongju National University (KNU/RM) for precipitation (PRCP)

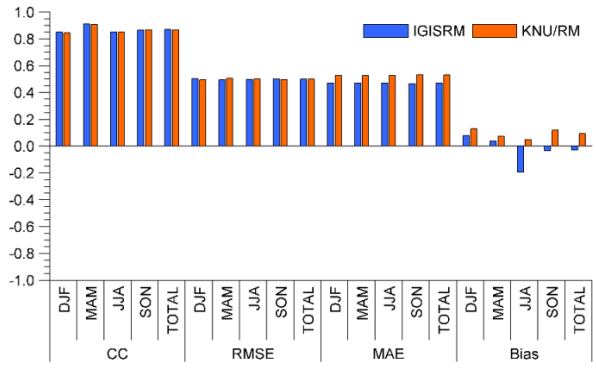

(a) PRCP

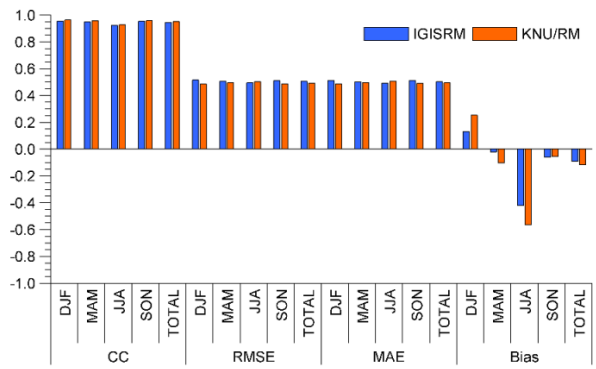

(b) TMAX

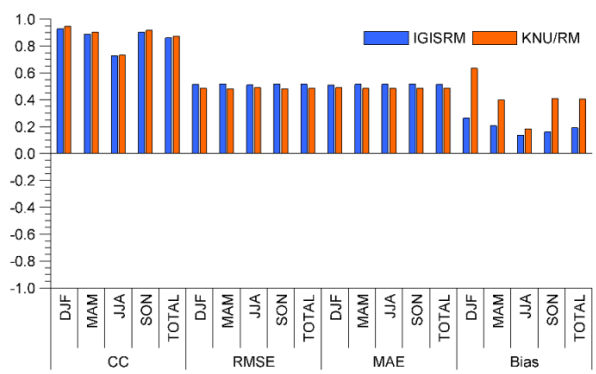

(c) TMIN

Figure 5.4 Inter-comparison of performance measures for precipitation (PRCP), maximum temperature (TMAX), and minimum temperature (TMIN) in December–February (DJF; winter), March–May (MAM; spring), June–August (JJA; summer), September–November (SON; autumn), and TOTAL (all time periods). The root-mean-square error (RMSE) was normalized for visualizing the graph.

IGISRM performed slightly better than KNU/RM in MAE and Bias for PRCP. The Bias in KNU/RM was lower than that in IGISRM for the summer season of June–August (JJA), in which large amounts of precipitation occur due to the monsoon and typhoons. However, the difference was not considerable. On the contrary, IGISRM performed better during other seasons; thus, the Bias of IGISRM during the total period was better. The TMAX, RMSE, and MAE of KNU/RM were lower than those of IGISRM. For TMIN, IGISRM performed better in Bias for all seasons and in the total period. Overall, the superiority between the two schemes was not clearly detected because large differences in CC, RMSE, and MAE between the two schemes were not observed for all variables; however, IGISRM showed considerable improvement in Bias for both TMIN and TMAX. Therefore, the five measures related to precipitation occurrence were evaluated to determine which technique provides more reliable and accurate climate information. The five measures averaged over all grid cells for all time periods are presented in Figure 5.5. The *FBias* of KNU/RM was above 1, which indicates that it predicts rainy points better than observation at AWSs; that of IGISRM was close to the perfect score of 1. Such a result is associated with the excessively longer radius of influence of KNU/RM applied to the overall grid cells in the domain because more stations far from a target grid cell may be included in the calculation of the probability of precipitation occurrence (POP). Such over-prediction of wet days affects the *H* score; consequently, KNU/RM had a higher *H* score. For other measures including *FAR*, *PC*, and *CSI*, however, IGISRM outperforms KNU/RM. In particular, FAR showed the largest difference between IGISRM and KNU/RM, which may have been induced by differences in the over-prediction of wet days between IGISRM and KNU/RM.

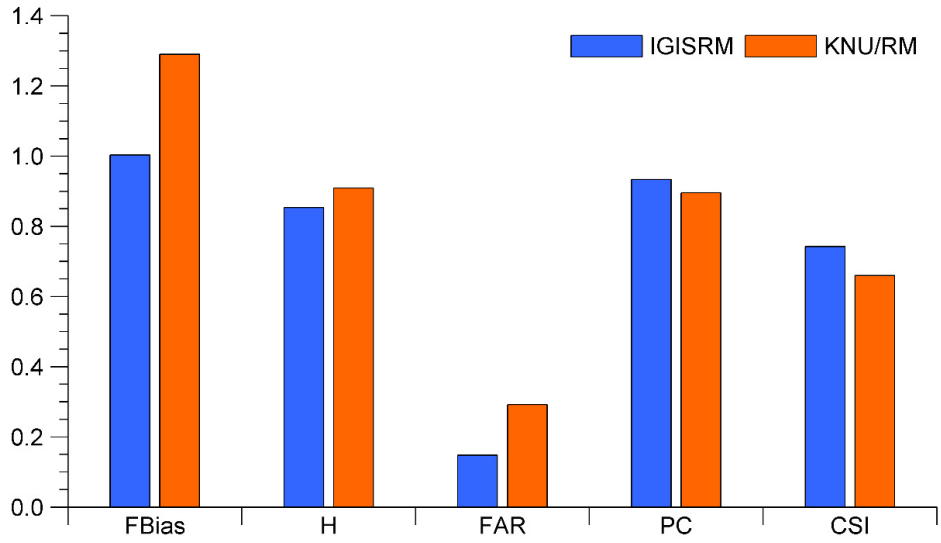

Figure 5.5 Inter-comparison of performance measures related to precipitation occurrence between the Improved GIS-based Regression Model (IGISRM) and the previous regression model of Kongju National University (KNU/RM)

This study also tested the skill in predicting precipitation occurrence by evaluating the performance for 10 precipitation cases showing different percentages of AWS station detecting rainfall, as shown in Table 5.2. A lower percentage of AWS station numbers detecting rainfall represents a lower continuity of precipitation occurrence, which indicates higher spatial variability in precipitation events. Five performance measures for the 10 cases are shown in Figure 5.6. KNU/RM showed an over-prediction of wet days, *FBias* > 1, in all cases, whereas IGISRM effectively predicted the precipitation occurrence, with values close to 1 from Case IV to Case X. In particular, KNU/RM showed extreme over-prediction of wet days in Case II, with 20% of AWSs detecting rainfall. Overall, IGISRM performs better than PRISM for all measures except the *H* score, whereas the two schemes showed compatible performances for high percentages of rainy stations (i.e., Case VIII to Case X). Interestingly, the performance of KNU/RM improved as the percentage increased from Case II to Case X, particularly for *FBias*, *FAR*, and *CSI*. Therefore, it is evident that the differences of all performance measures between IGISRM and KNU/RM for Case I to Case IV were significantly larger than those in other cases. This might have been induced by the higher spatial variability of precipitation occurrences in those cases. In particular, IGISRM prominently outperforms KNU/RM in Case II, which exhibited notably high spatial variability in precipitation occurrence. Figure 5.7 presents the spatial distribution of precipitation for observation, IGISRM and KNU/RM for July 18, 2008 (Case II). As expected, KNU/RM over-predicted wet areas, mostly represented by orange and yellow colors in the figure, whereas IGISRM showed good agreement with observation. Such results are strongly related to the differences in distance of R_p between IGISRM and KNU/RM. That is, KNU/RM used a longer R_p, which may have induced higher POP by including an excessive amount of rainy AWSs far from a target grid cell, consequently producing the drizzling effect. Such results indicate that IGISRM. with the radius of influence varying with station density, has better skill in capturing the spatial heterogeneity in precipitation occurrence on wet days.

The precipitation and temperature-related extreme climate indices listed in Table 5.3 were evaluated to determine which scheme produces more accurate information for extreme events. Figure 5.8 presents the correlation coefficient and K–S D statistics between observation and generated data at 236 AWSs from 2000 to 2010.

Table 5.2 Ten precipitation events selected on the basis of percentages of Automatic Weather Stations (AWSs) dectecting rainfall and the representative statistics of each event.

Case	Date (mm/dd/yyyy)	Number of station ≥ 1 mm/day	Rate (value in Col. 3/total number of stations × 100) (%)	Maximum rainfall (mm/day)	Average rainfall (mm/day)
I	04/18/2006	23	9.4	46.5	1.3
II	07/14/2008	47	19.2	33.5	1.6
III	08/08/2008	71	29.0	74.0	3.1
IV	08/08/2000	97	39.6	90.0	4.9
V	07/21/2002	118	48.2	202.5	12.0
VI	07/15/2009	144	58.8	211.0	33.2
VII	07/27/2006	164	66.9	203.0	53.1
VIII	06/12/2010	190	77.6	87.5	19.7
IX	07/07/2009	215	87.8	274.0	53.2
X	07/09/2009	236	96.3	246.0	89.2

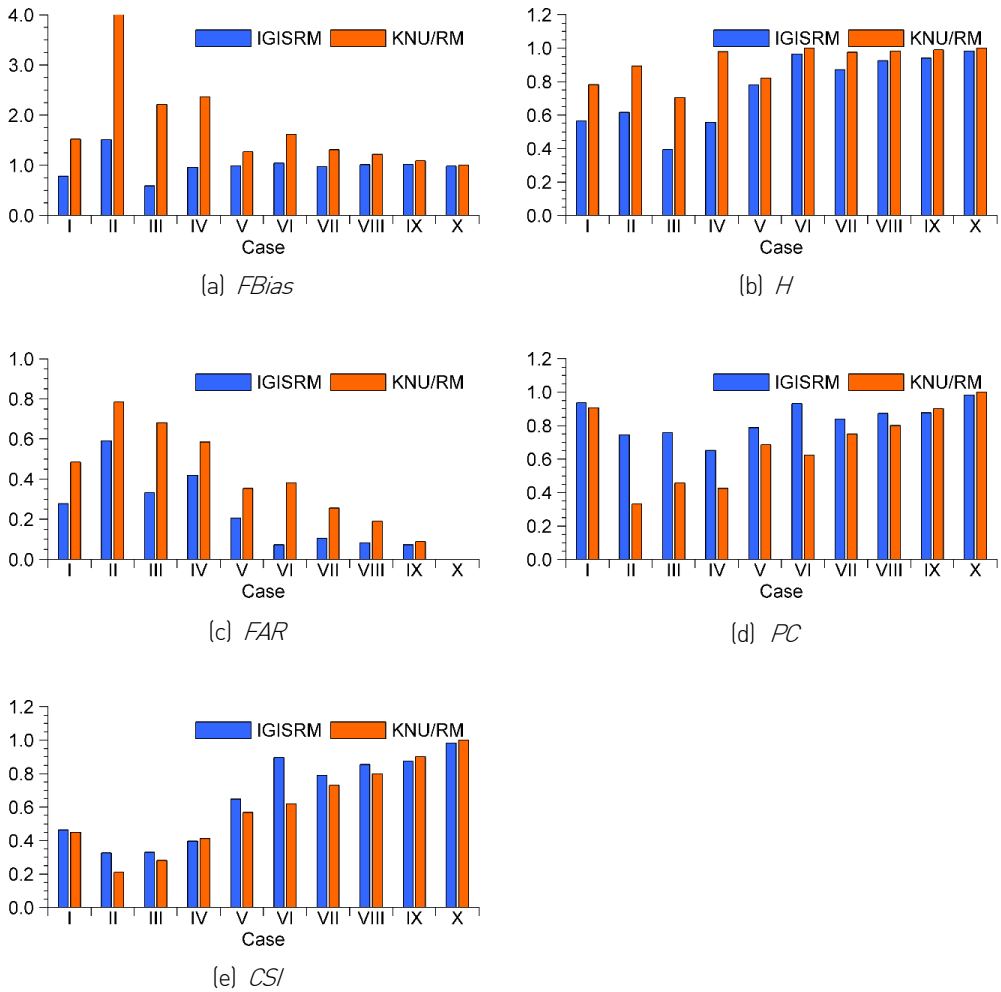

Figure 5.6 Performance measures of the Improved GIS-based Regression Model (IGISRM) and the previous regression model of Kongju National University (KNU/RM) for 10 cases selected on the basis of the percentages of Automatic Weather Stations (AWSs) detecting rainfall in South Korea

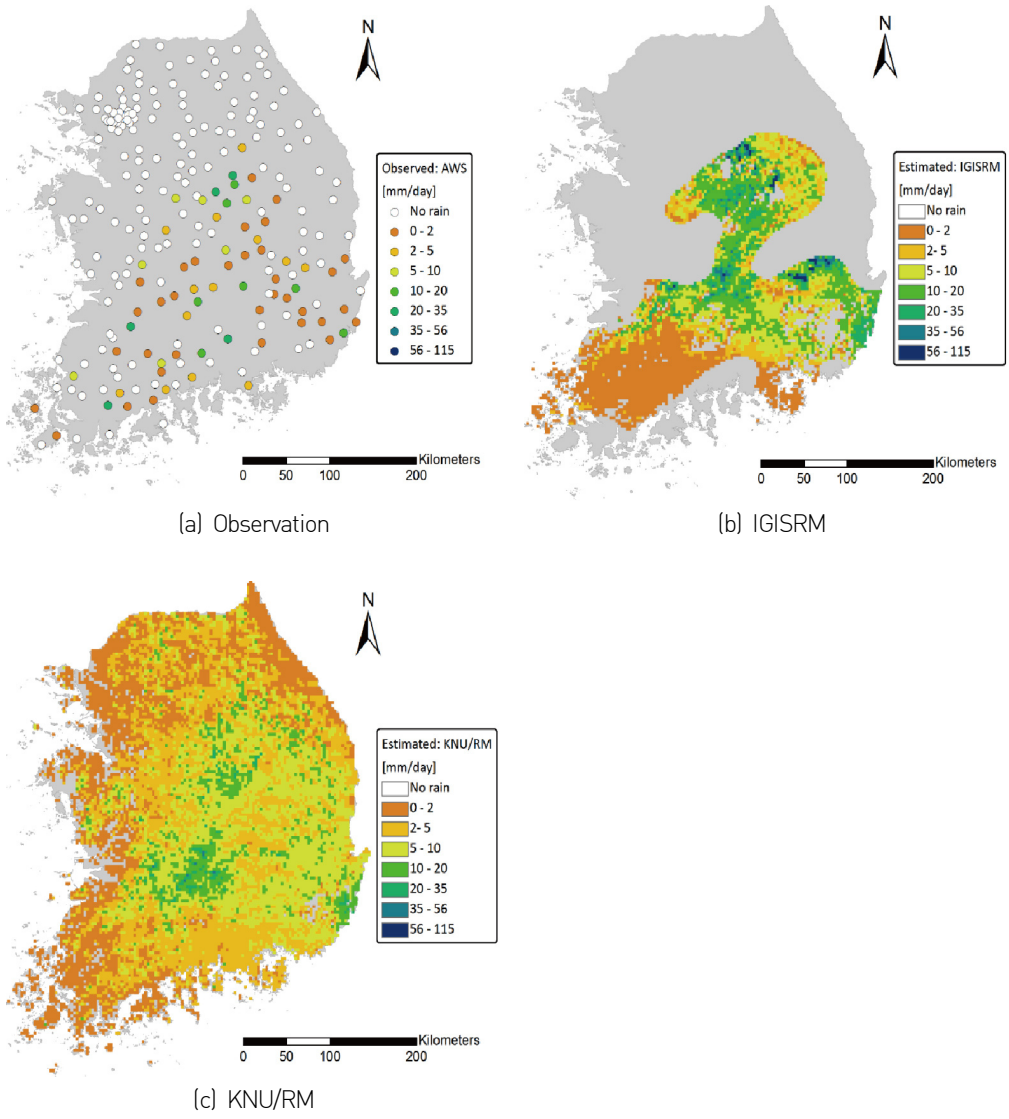

Figure 5.7 Spatial distributions of precipitation (PRCP) derived from observation, the Improved GIS-based Regression Model (IGISRM), and the previous regression model of Kongju National University (KNU/RM) on July 14, 2008 (Case II). The observed PRCP values are represented by point data at the Automatic Weather Stations (AWSs).

It should be noted that lower K–S D statistics [Figure 5.8(b)] represent better skill and that the values in Figure 5.8 represent the average of all AWSs. In addition, the first 16 indices, from CDD to SDII, indicate precipitation-related indices; those following indices SDII represent temperature-related indices. Notable differences in the correlation coefficient of the Gridded Temperature and Precipitation Climate Extremes Indices (CLIMDEX) between the two schemes are observed in the CDD and CWD indices, representing maximum lengths of dry and wet spells, respectively. These values are related to the skill in predicting precipitation occurrences. Because KNU/RM over-predicts wet days due to the longer R_p, it shows less skill in reproducing CDD and CWD with regard to the correlation coefficient compared with those of KNU/RM. However, no significant differences were detected for other CLIMDEX indices in the correlation coefficient. Regarding the K–S D statistics, the two schemes showed compatible skill for the temperature-related indices. However, IGISRM showed better skill for all precipitation-related indices, with lower K–S D statistics. In particular, significant differences were found in CDD, CWE, R01MM, and SDII. Such results may be closely related to the drizzling effect of KNU/RM, which may induce an excessive number of wet days with very small amounts of precipitation. For example, the R01MM index, representing the annual count of days when PRCP $\geq$ 1 mm, may have a much higher number compared with the observation owing to the drizzling effect in KNU/RM. In addition, SDII of KNU/RM showed relatively low values owing to the excessive number of wet days in a year. On the contrary, IGISRM, which introduced a varying influence radius by the iterative station density algorithm, showed better skill in CLIMDEX indices relative to precipitation occurrence.

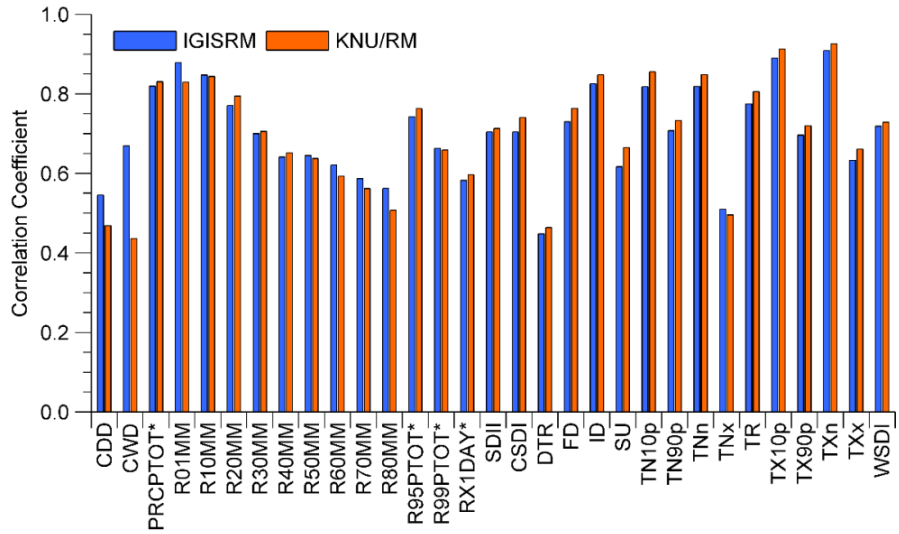

(a) Correlation coefficient

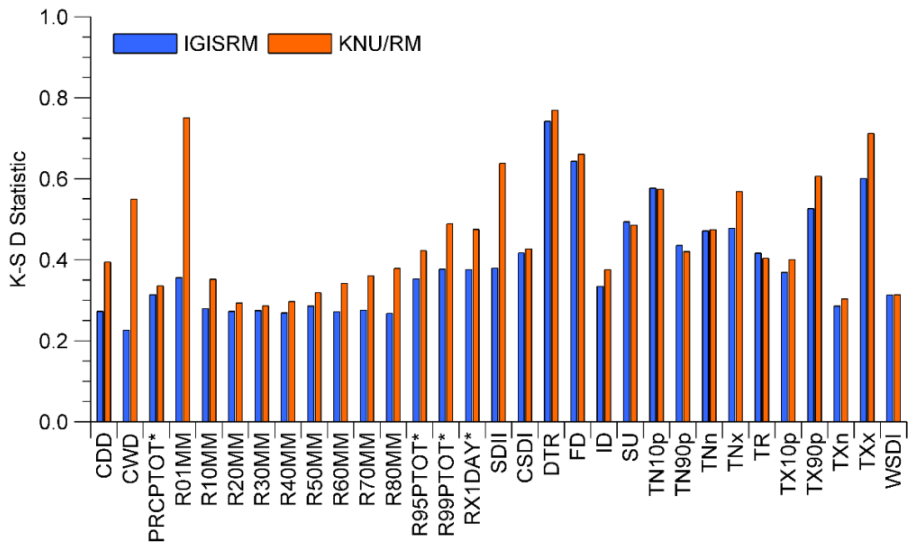

(b) K-S D statistics

Figure 5.8 Inter-comparison of performance on Gridded Temperature and Precipitation Climate Extremes Indices (CLIMDEX) between the Improved GIS-based Regression Model (IGISRM) and the previous regression model of Kongju National University (KNU/RM) based on the correlation coefficient and the Kolmogorov-Smirnov D (K-S D) statistic

5.4 Assessment of a suite of performance metrics for statistical downscaling methods

5.4.1 Sequencing of events

Seasonal correlations between the observed and downscaled CFSR datasets at 60 stations are shown in Table 5.3. The numbers in Table 5.3 represent the correlations averaged over all stations. All techniques were comparable for TMAX and TMIN, whereas SSI exhibited higher correlation for PRCP. This was particularly evident in JJA, which is affected by a monsoon climate. Such results indicate that the downscaling schemes do not provide substantial increases in skill for the sequencing of events. Moreover, they show that the CFSR reanalysis data provides high skill in the replication of day-to-day weather in the region. Among the four statistical downscaling models investigated in this study, BCSD showed slightly higher correlations. A comparison of BCCA and MACA revealed that MACA exhibits higher correlations for all variables and seasons, which indicates that introducing auxiliary variables into the constructed analog algorithm provides additional improvement in skill for daily climate sequences.

In addition, we investigated the spatial distributions of correlations over the study area. Because spatial variability of correlations in PRCP is lower than those of TMAX and TMIN, spatial maps of correlations for PRCP are presented. Figure 5.9 and Figure 5.10 show the spatial distribution of correlations of SSI and statistical downscaling methods for summer and winter seasons, respectively; that for other seasons is not shown. The correlations between the observed and downscaled datasets for summer at the south part in South Korea were lower than those at the north part.

Table 5.3 Seasonal correlations of daily sequences between observed and downscaled data sets. All values are averaged over 60 Automated Synoptic Observing System stations (ASOSs); bold values represent the best results.

Variable	Season	SSI	BCSD	BCCA	MACA	BCCI
TMAX	MAM	**0.950**	**0.950**	0.938	0.943	0.943
	JJA	0.857	0.868	0.837	0.850	**0.872**
	SON	**0.966**	0.964	0.955	0.958	0.952
	DJF	**0.912**	0.907	0.888	0.893	0.897
TMIN	MAM	0.845	**0.858**	0.849	0.857	0.855
	JJA	0.825	**0.847**	0.822	0.838	0.842
	SON	0.904	**0.915**	0.906	0.913	0.911
	DJF	**0.712**	0.707	0.684	0.694	0.699
PRCP	MAM	**0.614**	0.581	0.545	0.571	0.572
	JJA	**0.520**	0.485	0.430	0.462	0.485
	SON	0.623	0.606	0.553	0.579	**0.639**
	DJF	**0.617**	0.594	0.558	0.588	0.591

MAM: March to May (spring); JJF: June to August (summer); SON: September to November (autumn); DJF: December to February (winter)

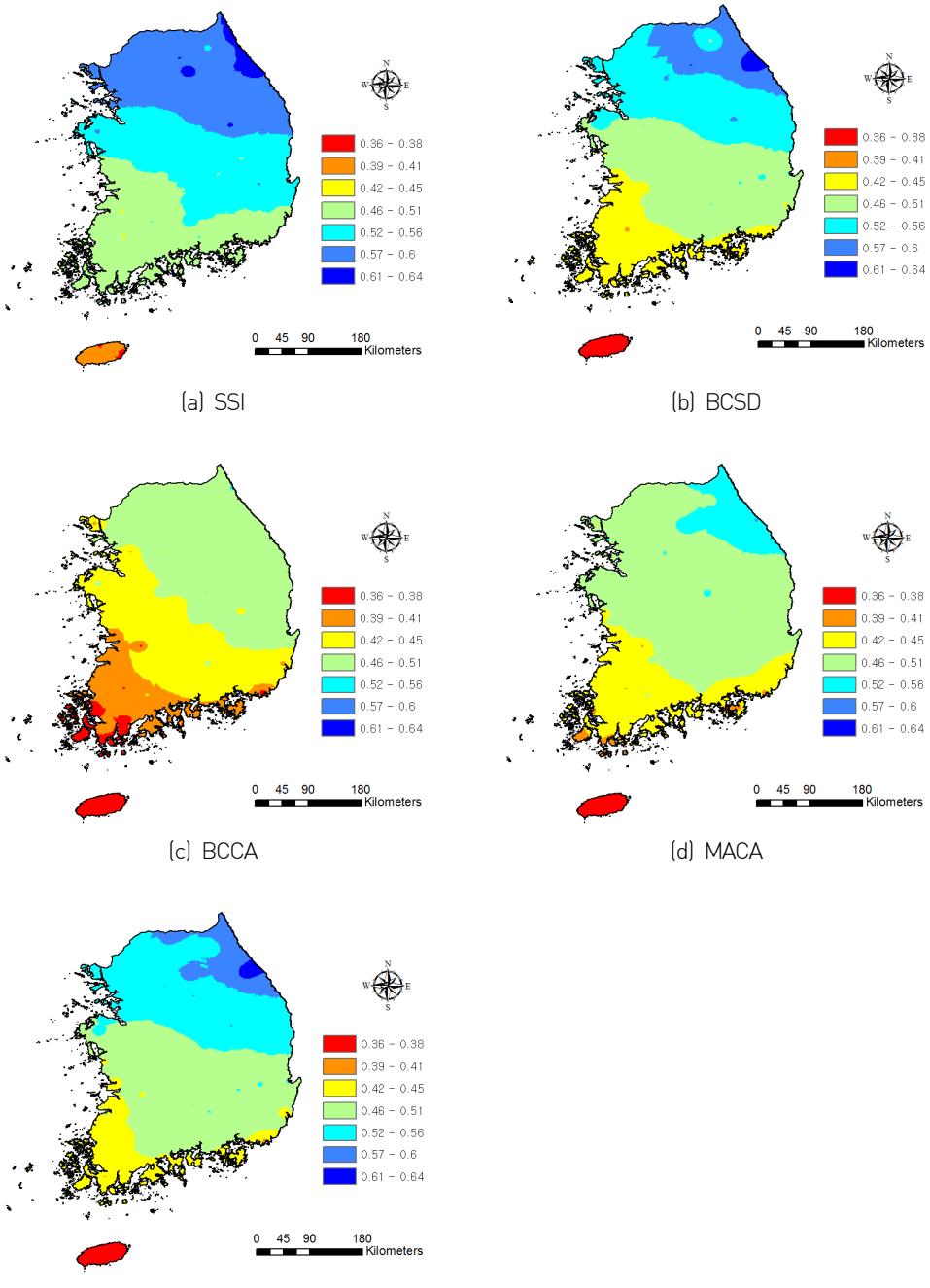

Figure 5.9 Spatial maps of correlation between the observed and downscaled Climate Forecast System Reanalysis (CFSR) precipitation datasets by simple spatial interpolation (SSI) and the four statistical downscaling methods employed in this study for the summer season (July–August, JJA) during the validation period

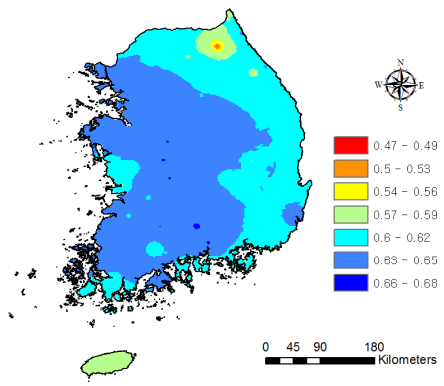

(a) SSI

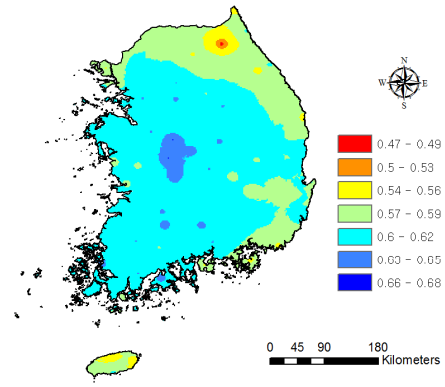

(b) BCSD

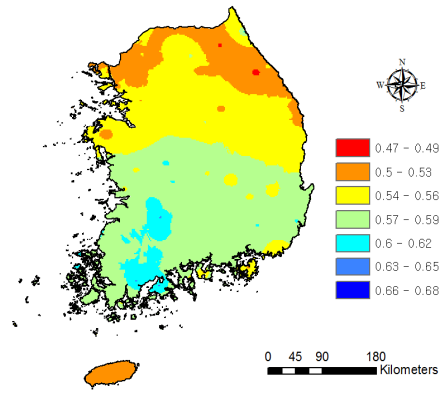

(c) BCCA

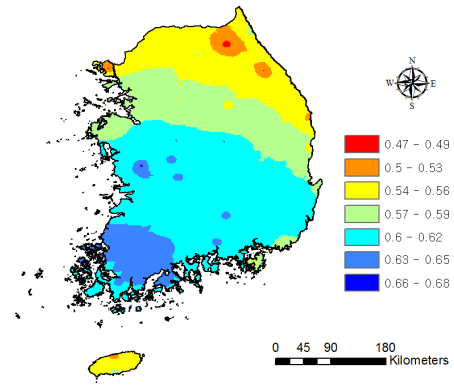

(d) MACA

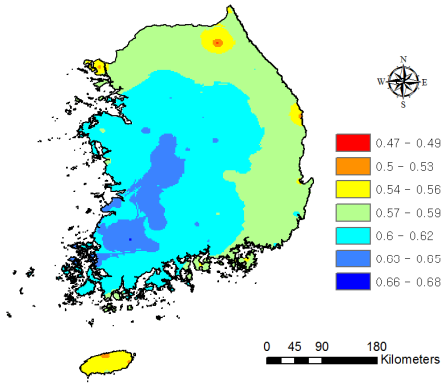

(e) BCCI

Figure 5.10 Same as Figure 5.8, but for the winter season (DJF)

Such results indicate that CFSR has less skill for summer precipitation at the south part owing to significant effects of typhoons, which are difficult to capture by CFSR. As expected, the spatial pattern of correlation for BCCA was similar to that of MACA, whereas while BCSD exhibited a spatial pattern similar to that of BCCI. On the contrary, the correlations at the south part for the winter season (Figure 5.10) were higher than those at the north part, likely because of combined effects of coarse spatial resolution of CFSR and measurement errors associated with snowfall and ice pellets at the north part during winter, particularly in the high-elevation mountainous areas at the northeastern part (Rinke et al., 2004; Neilsen et al., 2010; Eum et al., 2014).

Previous inter-comparison studies have shown that downscaling schemes such as BCSD, BCCA, and MACA improved daily correlation substantially compared with SSI based on North American Regional Reanalysis (NARR) (Mesinger et al., 2006) and NCEP/NCAR reanalysis datasets (Maurer and Hildalgo, 2008; Abatzoglou and Brown, 2012). The discrepancy between the results of those studies and the present study may be attributed to differences in sub-grid variables affected by regional characteristics such as topography and the reanalysis data to be downscaled.

5.4.2 Distribution of daily climate data

The skill of statistical downscaling methods in reproducing the distributions of observed daily climate data was evaluated by the K–S D statistic, which is defined as the maximum distance between CDFs of the observed and downscaled climate datasets. Therefore, a lower value of K–S D indicates better performance for this criterion.

The seasonal K–S D values are shown in Table 5.4; all values for correlation represent the averaged K–S D values over 60 stations. Compared with SSI, the K–S D values were improved considerably by the four downscaling models for winter and summer, at averages of 81% and 64%, respectively. Interestingly, the K–S D values for TMAX and TMIN during summer and winter were highest, representing the poorest performance among the four seasons. This suggests that CFSR lacks skill in capturing hot and cold extreme events. As expected, SSI showed the lowest

skill in simulating summer precipitation; the K–S D statistic improved by up to 93% by introducing the statistical downscaling models. BCSD and BCCI, which incorporate spatial disaggregation with quantile mapping bias correction, showed better skill in reproducing the distribution of station data than BCCA and MACA, which incorporate spatial weather analogs into the algorithms.

Because of the large improvement by the statistical downscaling models, higher spatial variability was noted for PRCP than TMAX and TMIN. Spatial maps of K–S D values from the four statistical downscaling models for summer precipitation, excluding SSI, are displayed in Figure 5.11. Similar to the results for correlation, the spatial patterns of K–S D statistics from BCSD and BCCI were similar, whereas BCCA was similar to MACA. In addition, all statistical downscaling models showed relatively poor performance at higher elevation regions in the northeast, which is likely attributed to the influence of orographic and complex topographic effects in this area.

Table 5.4 Seasonal Kolmogorov–Smirnov D (K–S D) statistics of the two-sample K–S test. All values were averaged over 60 Automated Synoptic Observing System (ASOS) sites. Lower values represent better skill; bold values represent the best results among the five downscaling techniques.

Variable	Season	SSI	BCSD	BCCA	MACA	BCCI
TMAX	MAM	0.195	**0.051**	0.053	0.053	0.053
	JJA	0.279	0.053	**0.052**	**0.052**	**0.052**
	SON	0.165	**0.044**	0.045	0.045	0.045
	DJF	0.188	**0.094**	0.097	0.097	0.099
TMIN	MAM	0.119	**0.054**	0.055	0.055	0.056
	JJA	0.174	**0.053**	**0.053**	0.054	**0.053**
	SON	0.122	**0.053**	0.054	0.054	**0.053**
	DJF	0.216	**0.099**	0.101	0.101	0.102
PRCP	MAM	0.276	0.020	**0.019**	0.020	**0.019**
	JJA	0.379	**0.027**	0.028	0.028	**0.027**
	SON	0.303	**0.022**	0.023	0.023	0.023
	DJF	0.353	0.034	**0.033**	**0.033**	**0.033**

MAM: March to May (spring); JJF: June to August (summer); SON: September to November (autumn); DJF: December to February (winter)

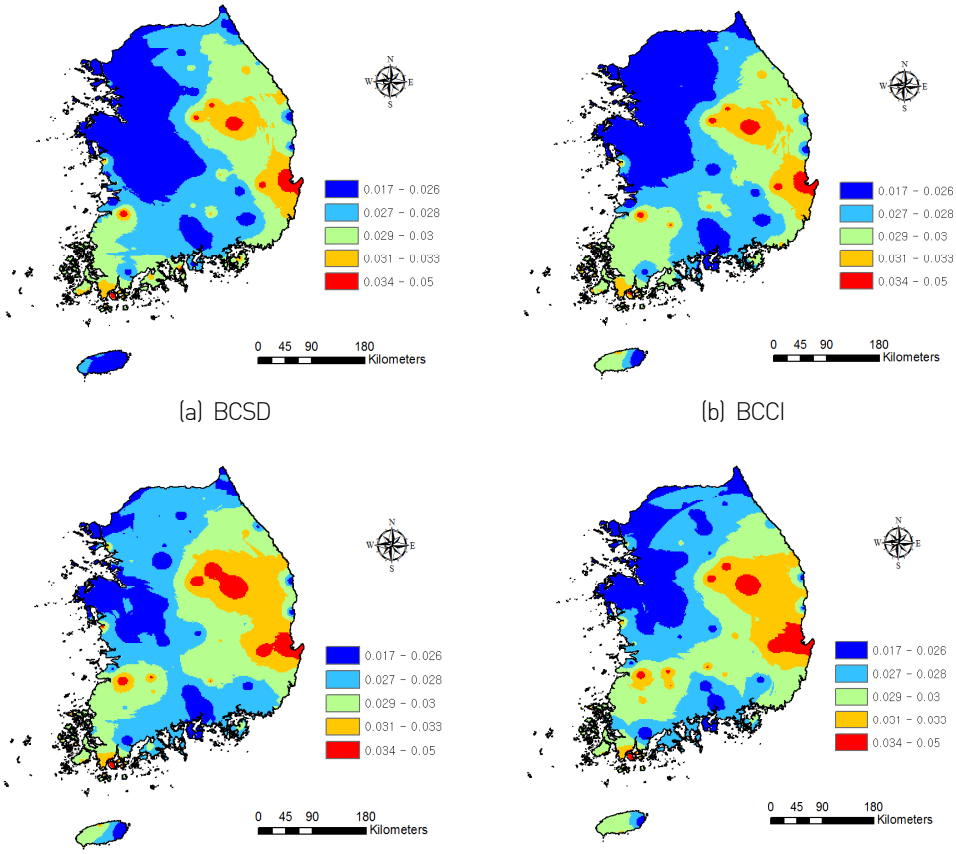

Figure 5.11 Spatial maps of the Kolmogorov–Smirnov D (K–S) D statistic from the four statistical downscaling methods for summer precipitation during the validation period

5.4.3 Spatial correlations between stations

The third metric measures the ability of methods in reproducing spatial correlation, which is an important factor when simulating hydrologic responses for water resource management. The RMSEs of spatial correlations between the observed and downscaled datasets are shown in Table 5.5. The RMSEs for SSI during summer for all variables were higher than those during other seasons, which may be attributed to the localized nature of heat waves and heavy rainfall during summer. However, the RMSEs were considerably reduced by the downscaling methods. In particular, large improvements by BCCA and MACA were found for all variables, up to 45% on average by MACA for PRCP versus 8% for BCCI. An important finding is that the spatial structure of summer precipitation was improved by MACA. Because summer precipitation, as indicated above, is significantly affected by typhoons, leading to localized heavy rainfall under a monsoon climate, it is difficult to capture the spatial structure over the study area. Moreover, approximately 60% of the annual precipitation occurs during summer. This has significant implications for water resource management because a balance must be kept between maintaining the water supply during drawdown period in spring, autumn, and winter and flood prevention during summer (Eum et al., 2011).

Figure 5.12 displays scatter plots of the spatial correlations for PRCP of summer and winter during the calibration period. For summer precipitation, SSI and BCCI overestimated the spatial correlations owing to the intrinsic bias of CFSR, whereas MACA was concentrated near the 1:1 line. For winter precipitation, all statistical downscaling models showed comparable levels of performance, although SSI and BCSD tended to overestimate the spatial correlations.

Table 5.5 Root–mean–square errors (RMSEs) of seasonal spatial correlations among stations for observed and downscaled datasets. All values were averaged over 60 Automated Synoptic Observing System (ASOS) sites. Bold values represent the best results among the five downscaling techniques.

Variable	Season	SSI	BCSD	BCCA	MACA	BCCI
TMAX	MAM	0.054	0.047	**0.025**	0.028	0.057
	JJA	0.124	0.099	0.059	**0.053**	0.115
	SON	0.028	0.024	**0.010**	0.012	0.030
	DJF	0.052	0.049	**0.024**	0.029	0.058
TMIN	MAM	0.055	0.045	0.028	**0.026**	0.056
	JJA	0.137	0.051	0.056	**0.033**	0.053
	SON	0.049	0.023	0.027	**0.016**	0.021
	DJF	0.106	0.103	**0.048**	0.057	0.114
PRCP	MAM	0.108	0.087	0.089	**0.067**	0.096
	JJA	0.152	0.124	**0.067**	0.068	0.153
	SON	0.136	0.094	0.099	**0.076**	0.126
	DJF	0.108	0.094	0.100	**0.061**	0.091

MAM: March to May (spring); JJF: June to August (summer); SON: September to November (autumn); DJF: December to February (winter)

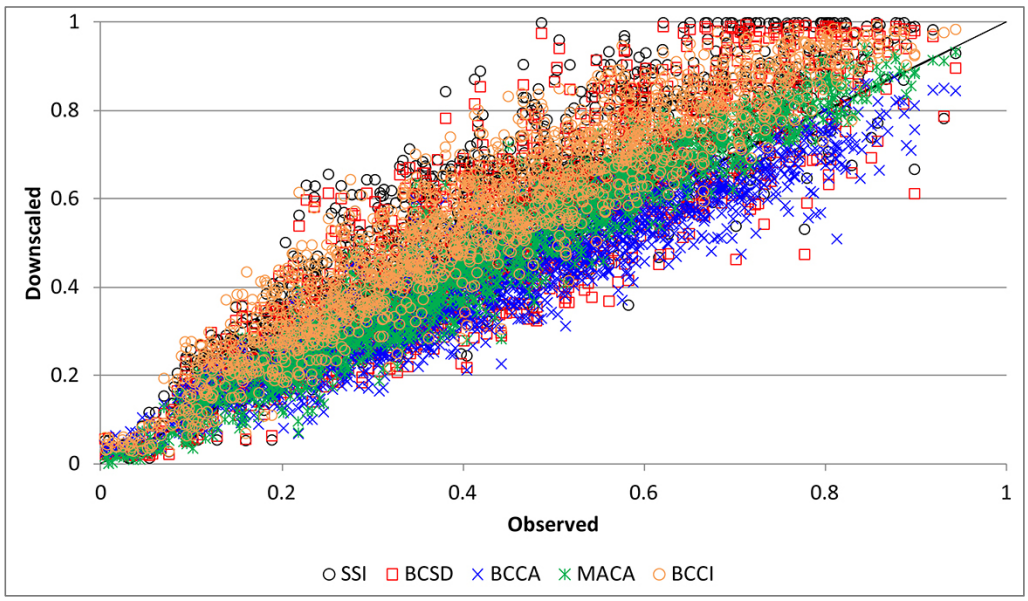

(a) Summer

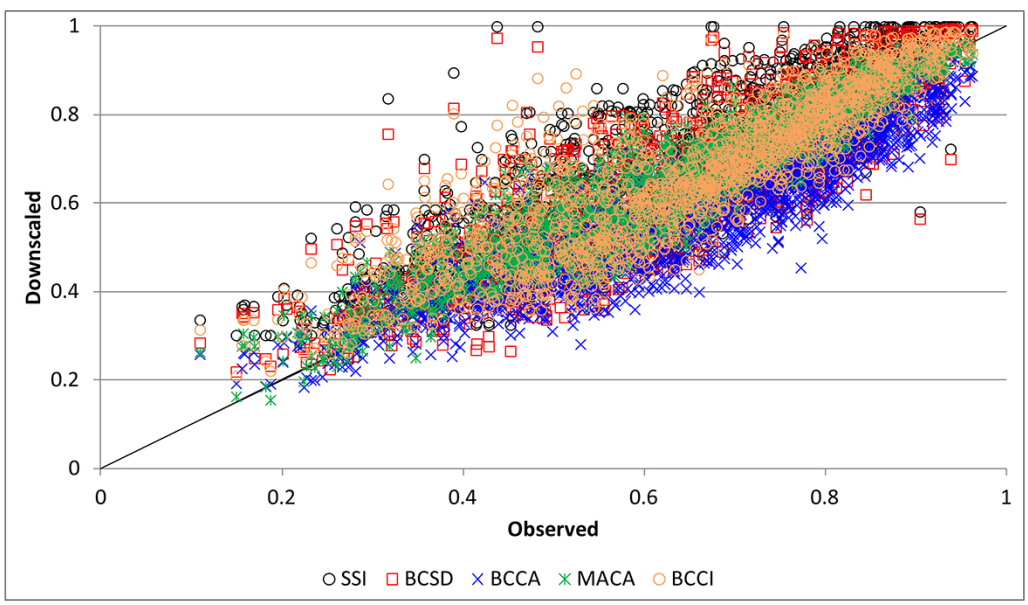

(b) Winter

Figure 5.12 Scatter plots of spatial correlations among stations from all methods for summer (upper) and winter (lower) precipitation during the validation period. Dots falling on the 45° line indicate perfect simulation.

Overall, the methods incorporating spatial weather patterns, BCCA and MACA, provided more accurate spatial structure of PRCP, TMAX, and TMIN, whereas SSI, BCSD, and BCCI, which rely on spatial interpolation schemes, tended to overestimate the spatial correlations.

5.4.4 Extremes

The fourth performance criterion measures the ability of the statistical downscaling models in simulating extreme events. The performance was measured by the proportion of stations passing the two-sample K–S test at the 5% significance level for the 23 ETCCDI indices. Table 5.6 shows the proportion of passed K-S tests for each ETCCDI index. The performance on extreme indices related to TMIN was generally better than that for TMAX. PRCP-related indices with the highest proportion of passed tests by SSI corresponded to the same results as those for the statistical downscaling models, indicating that the downscaling performance is highly dependent on the skill of CFSR. In general, it was determined that CFSR reproduces observed PRCP extremes well, particularly for consecutive no-rainfall days (CDD) and annual precipitation (PRCPTOT). Despite the high baseline, the performance was improved by the statistical downscaling models relative to SSI. Based on the average proportion of passed tests for each variable, BCSD, BCCA, and BCCI showed the best performance for TMAX, TMIN, and PRCP, respectively. Averaged over all ETCCDI indices, BCSD showed the highest skill in simulating extremes. This may be related to its performance on the distribution metric reported earlier because the maximum differences among distributions often occur at the most extreme values.

Table 5.6 Proportions of stations passing the K–S test at the 5% significance level for the 23 Expert Team on Climate Change Detection and Indices (ETCCDI) values categorized according to their relation with TMAX, TMIN, and PRCP. Bold values represent the best results among the five downscaling techniques on average.

Variable	Indices	SSI	BCSD	BCCA	MACA	BCCI
TMAX	SU	0.050	0.933	0.900	0.883	0.933
	ID	0.333	0.267	0.283	0.250	0.283
	TXx	0.150	0.933	0.950	0.967	0.933
	TXn	0.500	0.533	0.400	0.400	0.433
	TX10	0.000	0.517	0.367	0.417	0.417
	TX90	0.017	0.633	0.667	0.683	0.633
	WSDI	1.000	1.000	1.000	1.000	1.000
	DTR	0.067	0.500	0.517	0.550	0.517
Average		0.265	**0.665**	0.635	0.644	0.644
TMIN	FD	0.317	0.750	0.700	0.717	0.700
	TR	0.283	0.917	0.867	0.900	0.883
	TNx	0.200	0.667	0.850	0.783	0.800
	TNn	0.383	0.617	0.517	0.467	0.550
	TN10	0.250	0.283	0.317	0.317	0.350
	TN90	0.333	0.733	0.750	0.700	0.750
	CSDI	0.600	0.800	0.850	0.850	0.767
	DTR	0.067	0.500	0.517	0.550	0.517
Average		0.304	0.658	**0.671**	0.660	0.665
PRCP	RX_1DAY	0.317	1.000	0.983	0.983	0.983
	RX_5DAY	0.567	1.000	0.967	0.950	1.000
	SDII	0.017	0.967	1.000	0.983	0.983
	OCDD	0.883	1.000	1.000	1.000	1.000
	OCWD	0.250	1.000	1.000	1.000	1.000
	R95pTOT	0.217	0.967	0.983	0.983	1.000
	R99pTOT	0.383	1.000	1.000	1.000	1.000
	PRCPTOT	0.833	1.000	0.983	1.000	1.000
Average		0.433	0.992	0.990	0.987	**0.996**

PRCPTOT is often used as an index for categorizing climatologically wet and dry areas. The annual maximum difference between TMAX and TMIN (DTR) is the only index related to both TMAX and TMIN. Figures 5.13 and 5.14 show the spatial distributions of mean PRCPTOT and DTR, respectively, during the calibration period for observations and all statistical downscaling models used in this study. SSI underestimated PRCPTOP over South Korea, whereas the other four methods showed good agreement with the observations, particularly in the southeast. However, the statistical downscaling models underestimated PRCPTOT at the central and northern areas. Regarding DTR, the four methods show very good agreement with the spatial distribution of the observations. However, SSI strongly underestimated DTR except over the southernmost Jeju Island. In addition, the time series of the spatially averaged extreme indices showed poor skill by SSI but large increases in the proportion of passed tests when the downscaling methods were applied. Figure 5.15 a displays time series of indices related to TMAX, including SU, TXx, TXn, and TX90. SSI had a cold bias and underestimated all extreme indices, mainly resulting from the coarse grid size that simultaneously includes ocean and land data. For example, the annual maximum values of TMAX (TXx) were underestimated 2.7°C on average by SSI, whereas the four methods removed the bias to show large improvement in TXx. For extreme indices related to TMIN (Figure 5.16), SSI had a warm bias, leading to underestimation of FD and TNx and overestimation of TNn and TN90. Again, downscaling largely removed this bias.

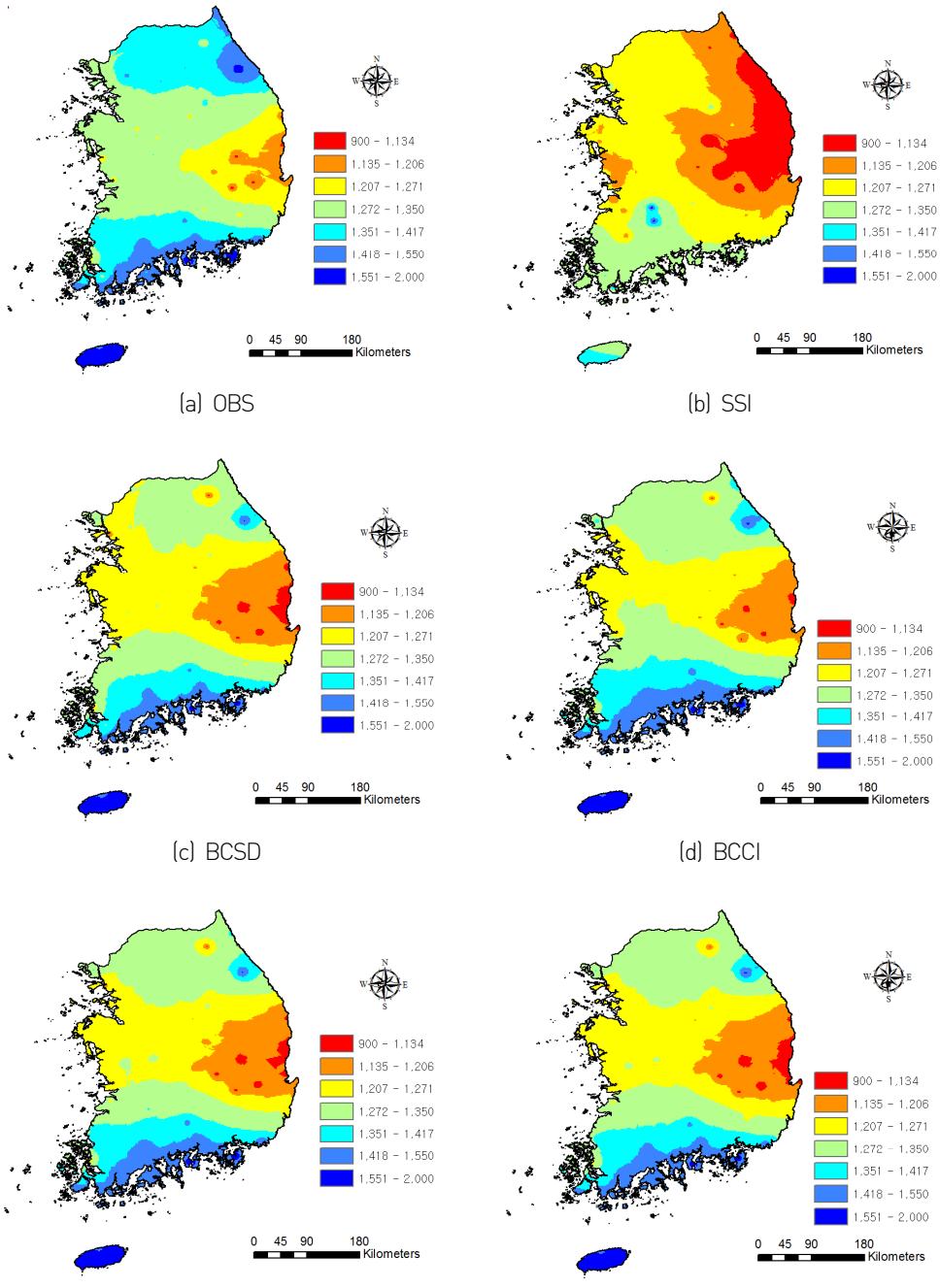

Figure 5.13 Spatial distributions of mean annual precipitation (PRCPTOT) from the observations (Obs), simple spatial interpolation (SSI), and the four downscaling methods used during the validation period

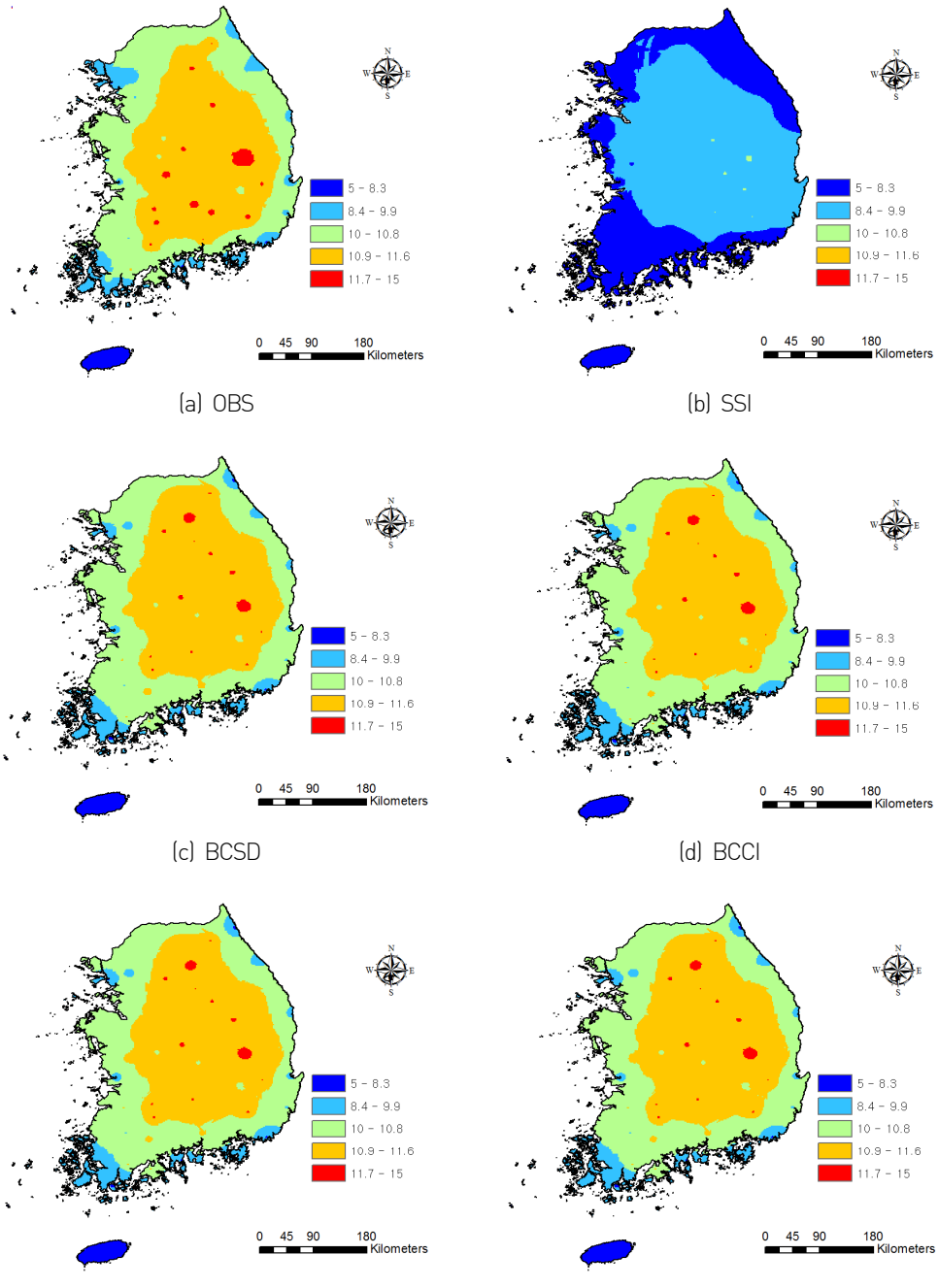

Figure 5.14 Same as Figure 5.13, but for the mean annual maximum difference between daily maximum and minimum temperature (DTR)

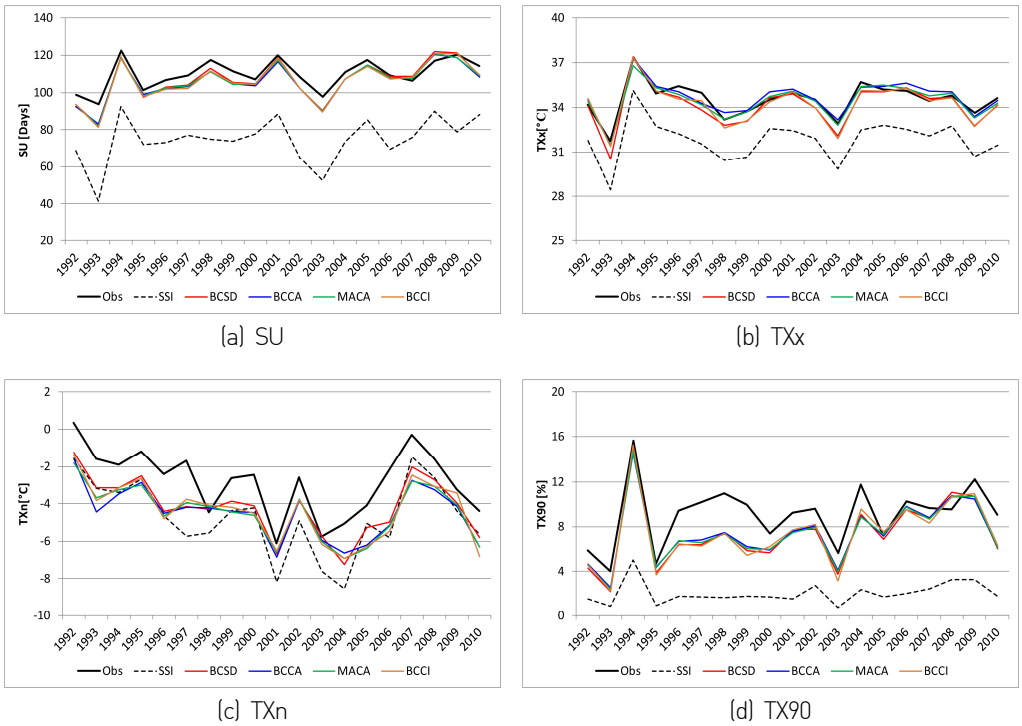

(a) SU (b) TXx

(c) TXn (d) TX90

Figure 5.15 Time series of selected extreme indices related to maximum temperature (TMAX) during the validation period from 1992 to 2010

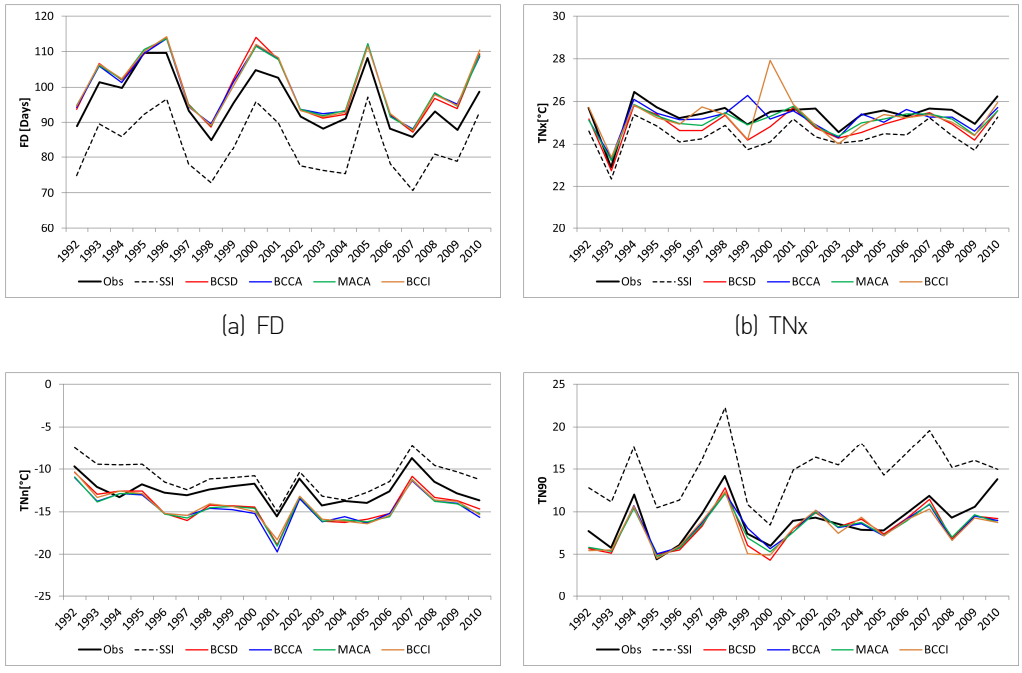

(a) FD (b) TNx

(c) TNn (d) TN90

Figure 5.16 Same as Figure 5.15, but for extreme indices related to minimum temperature (TMIN)

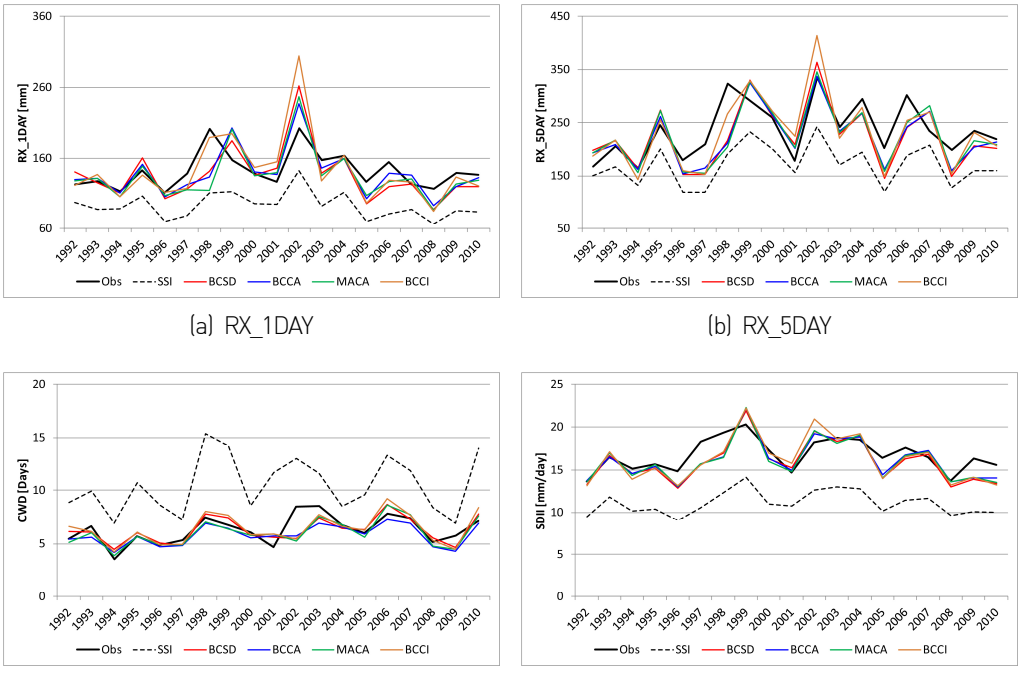

(a) RX_1DAY (b) RX_5DAY

(c) CWD (d) SDII

Figure 5.17 Same as Figure 5.15, but for extreme indices related to precipitation (PRCP).

Figure 5.17 shows a time series of precipitation related extreme indices including RX_1DAY, RX_5DAY, CWD, and SDII. SSI underestimated RX_1DAY and RX_5DAY, likely owing to the inability of CFSR in capturing topographic effects on precipitation by CFSR. However, CWD was overestimated by SSI, indicating more wet days owing to the ocean effects within CFSR grid cells. In addition, SSI underestimated SDII, the precipitation intensity per day, which may be related to a drizzling bias in CFSR precipitation fields. As indicated in Table 5.6, all indices were significantly improved by the statistical downscaling methods used in this study.

5.5 Identifying robust statistical downscaling models with TOPSIS

In previous sections, each method showed different levels of skill on each performance metric. Selecting a preferred technique when considering a single metric is straight-forward. In general, however, multiple criteria should be considered because accurate simulation of hydrologic and ecological responses depend on all of the metrics considered in this study. Therefore, the use of a systematic procedure for identifying a robust downscaling model using the TOPSIS technique is suggested.

Table 5.7 shows the ranking of the four methods based on the performance metrics suggested in this study. In the table, preference is given to the method showing the highest average ranking with the smallest standard deviation, i.e., that representing high and stable skill over all seasons. For TMAX, MACA and BCCA had the same priority with the same average ranking and standard deviation, which means that either method can robustly downscale TMAX for the study area. MACA also showed the highest ranking for TMIN, and BCCA is the second prioritized alternative.

Table 5.7 Ranking of the four statistical downscaling methods with the Technique for Order of Preference by Similarity to Ideal Solution (TOPSIS) technique based on the comprehensive performance metrics evaluated in this study

Variable	Season	BCSD	BCCI	BCCA	MACA
TMAX	MAM	3	4	1	2
	JJA	3	4	2	1
	SON	3	4	2	1
	DJF	3	4	1	2
	Avg.	3.0	4.0	1.5	1.5
	Std.	0.0	0.0	0.6	0.6
TMIN	MAM	3	4	2	1
	JJA	3	4	1	2
	SON	3	4	2	1
	DJF	3	4	2	1
	Avg.	3.0	4.0	1.8	1.3
	Std.	0.0	0.0	0.5	0.5
PRCP	MAM	2	4	3	1
	JJA	3	4	2	1
	SON	2	4	3	1
	DJF	3	2	4	1
	Avg.	2.5	3.5	3.0	1.0
	Std.	0.6	1.0	0.8	0.0

MAM: March to May (spring); JJF: June to August (summer); SON: September to November (autumn); DJF: December to February (winter)

These results indicate that methods incorporating spatial weather patterns are well-suited to downscaling TMAX and TMIN. MACA is also a top-ranked method for PRCP over all seasons, with BCSD recommended as the second-best alternative owing to its skill in simulating distributions and extremes. Overall, MACA was found to be the most reliable and robust method for TMAX, TMIN, and PRCP in South Korea, whereas BCCI is the least recommended, owing mainly to poor skill in simulating the spatial structure (Table 5.5). A comparison of BCCA and MACA indicated that MACA had better or comparable skill for all variables and seasons, indicating that the introduction of auxiliary variables to improve coherence of the analogs leads to added downscaling. Because MACA requires additional variables as predictors, BCCA and BCSD can be considered as second alternatives for TMAX and TMIN, and PRCP, respectively, when only TMAX, TMIN, and PRCP fields are available as predictors.

6. CONCLUDING REMARKS

In this study, IGISRM is suggested because it introduces the iterative station density algorithm into the structure of KNU/RM to incorporate R_p, which varies with the station density near a target grid. The performances of IGISRM at various spatial resolutions are evaluated to select a suitable spatial resolution with regard to accuracy and computational efficiency. By using IGISRM, a long-term gridded climate dataset from 1973 to 2010 can be generated for regional applications. In addition, inter-comparison of the performances between IGISRM and KNU/RM is implemented to evaluate the performance measures related to the amount of each variable and precipitation occurrence and to the ETCCDI values to examine its ability to reproduce extreme climate events.

The results show that the iterative station density algorithm in IGISRM properly reflects the station density near each grid cell in the calculation of R_p. Among five spatial resolution tested in this study, 3 km resolution is shown to properly produce a long-term gridded climate dataset with regard to the performance measures and total number of grid cells to be interpolated. The current station spacing for ASOS sites over South Korea is about 40 km; that for AWSs is 12 km. The performance of IGISRM might be varied with degrees of station density; that is, the accuracy of AWS might be improved by employing AWSs into the IGISRM. Therefore, an optimal station network to maximize the performance and to minimize the number of stations can be detected by adding stations in areas of low station density. In addition, the optimal grid-spacing selected in this study can be changed when employing more observational stations into the IGISRM procedure. Both IGISRM and KNU/RM show compatible performances in the performance measures related to the amount of each variable. However, IGISRM shows better skill in Bias for TMIN and outperforms KNU/RM for all performance measures related to precipitation occurrence. In particular, IGISRM produces better spatial distribution of precipitation when the spatial variability in the precipitation occurrence is higher, such as Case II to Case IV. Such results indicate that IGISRM can provide better skill in capturing the spatial heterogeneity in precipitation occurrence. Although the two schemes show the compatible skill for the temperature-related CLIMDEX values, IGISRM shows higher skill in reproducing CDD, CWE, R01MM, and SDII. These indices are closely related

to the drizzling effect of KNU/RM due to the longer R_d, which induces an excessive number of wet days over the domain.

Regarding statistical downscaling methods, MOS-based statistical downscaling methods have been developed and are successfully used to downscale the outputs of GCMs to a local scale. Four methods widely used in various fields—BCSD, BCCI, BCCA, and MACA—as well as SSI as a surrogate downscaling scheme for measuring the skill of CFSR, have been evaluated in terms of sequencing of events, distribution, spatial structure, and extremes. PRCP, TMAX, and TMIN from CFSR are downscaled to stations over South Korea. By dividing historical observational station data into two parts, all statistical downscaling models are calibrated with 19 years of data from 1973 to 1991 and are validated with 19 years from 1992 to 2010. On the basis of the four performance metrics, the TOPSIS technique is employed to identify robust methods for the study area.

Owing to the high correlations among surface observations and CFSR, statistical downscaling methods do not show substantial increases in skill at sequencing events. Regarding the skill for replicating observed distributions of climate variables, K–S D statistics show considerable improvement by using the statistical downscaling methods. BCSD and BCCI show slightly better skill in reproducing the distribution of station data than BCCA and MACA. In addition, all methods show lower skill at higher elevation stations, where more extremes are influenced by orographic effects and complex topography. In terms of spatial structure, BCCA and MACA outperform BCSD and BCCI mainly because they incorporate spatial weather patterns into the downscaling process. In particular, MACA shows large increases in skill for summer precipitation. For climate extremes, SSI shows the highest proportion of passed tests for PRCP. These proportions show considerably improvement when using the statistical downscaling methods. In particular, the warm, cold, and wet biases of SSI are removed for TMAX, TMIN, and PRCP, respectively. Averaged over all variables, BCSD shows the highest skill in simulating the 23 ETCCDI values. On the basis of the TOPSIS analysis, MACA is shown to be the most reliable and robust method for all variables in South Korea, whereas BCCI shows the poorest performance, mainly stemming from its poor skill in simulating spatial structure. In addition, MACA's use of auxiliary variables results in added values compared with BCCA.

This study has developed a long-term gridded climate dataset and multiple statistical downscaling methods. Climate variables downscaled to a gridded climate dataset may be useful for distributed hydrologic models that require input data on a regular grid. Therefore, a straightforward next step might be downscaling GCMs to the gridded data at 3 km resolution by the statistical downscaling methods developed in this study. Moreover, recent studies have focused on 21st century downscaled climate change projections based on the CMIP5 (Maloney et al. 2014). As one of the first downscaling inter-comparison studies for South Korea, we have downscaled CFSR data to a network of stations and have ranked the downscaling skill by using TOPSIS. Rather than a single CFSR, downscaling CMIP5 climate scenarios with the four statistical downscaling methods might result in different rankings of the statistical downscaling methods based on same performance measures. Moreover, studies have raised potentially serious issues with bias-correction techniques such as quantile mapping, which is used in BCSD, BCCI, BCCA, and MACA, regarding the preservation of long-term projected trends from the driving GCMs (Maraun, 2013; Maurer and Pierce, 2014). In response, various algorithms have been developed to preserve the long-term trend of climate projections such as equidistant quantile matching (Li et al., 2010), the ISI-MIP approach (Hempel et al., 2013), detrended quantile mapping (Bürger et al., 2013), and quantile delta mapping (Cannon et al., 2015). Employment of such a new bias correction technique with the methods recommended in this study can be used to downscale various CMIP5 projections for regional applications to climate change impact studies in South Korea.

REFERENCES

Abatzoglou, J.T., and T.J. Brown, 2011: A comparison of statistical downscaling methods suited for wildfire applications. International Journal of Climatology, 32, 772-780, doi:10.1002/joc.2312.

Awasthi, A., S.S. Chauhan, and H. Omrani, 2011: Application of fuzzy TOPSIS in evaluating sustainable transportation systems. Expert System with Applications, 38 (10), 12270-12280.

Bardossy, A., I. Bogardi, and I. Matyasovszky, 2005: Fuzzy rule-based downscaling of precipitation. Theoretical and Applied Climatology, 82, 119-129.

Barsugli, J.J., G. Guentchev, R.M. Horton, A. Wood, L.O. Mearns, X.-Z. Liang, J.A. Winkler, K. Dixon, K. Hayhoe, R.B. Rood, L. Goddard, A. Ray, L. Buja, and C. Ammann, 2013: The Practitioner's Dilemma: How to assess the credibility of downscaled climate projections, Eos Transitions AGU, 94 (46), 424-425, doi:10.1002/2013EO460005.

Barry, R.G., and R.J. Chorley, 1987: Atmosphere, weather, and climate. 5th ed. Routledge, London, United Kingdom, 460 p.

Bennett, K., A.T. Werner, and M. Schnorbus, 2012: Uncertainties in hydrologic and climate change impacts analyses in headwater basins of British Columbia. Journal of Climate, 25, 5711-5730.

Boer, E.P.J., K.M. Beurs, and A.D. Hartkamp, 2001: Kriging and thin plate splines for mapping climate variables. International Journal of Applied Earth Observation and Geoinformation, 3, 146-154.

Brekke, L.D., J.E. Kiang, J.R. Olsen, R.S. Pulwarty, D.A. Raff, D.P. Turnipseed, R.S. Webb, and K.D. White, 2009: Climate change and water resources management—A federal perspective, U.S. Geological Survey Circular, 1331, 65 p. [Available at http://pubs.usgs.gov/circ/1331/.]

Brekke, L., B.L. Thrasher, E.P. Maurer, and T. Pruitt, 2013: Downscaled CMIP3 and CMIP5 Climate Projections: Release of Downscaled CMIP5 Climate Projections [Available at http://gdo-dcp.ucllnl.org/downscaled_cmip_projections/].

Bürger, G., T.Q. Murdock, A,T. Werner, S.R. Sobie, and A.J. Cannon, 2013: Downscaling extremes—An intercomparison of multiple statistical methods for present climate. Journal of Climate, 25(12), 4366-4388.

Butt, N., P.A. De Oliveira, and M.H. Costa, 2011: Evidence that deforestation affects the

onset of the rainy season in Rondonia, Brazil. Journal of Geophysical Research, 116 (11), doi:10.1029/2010JD015174.

Cannon, A.J., S.R. Sobie, and T.Q. Murdock, 2015: Bias correction of GCM precipitation by quantile mapping: How well do methods preserve changes in quantiles and extremes? Journal of Climate, 28, 6938-6959.

Chen, J., F.P. Brissette, and R. Leconte, 2011: Uncertainty of downscaling method in quantifying the impact of climate change on hydrology. Journal of Hydrology, 401, 190-202.

Cherubini, T., A. Ghelli, and F. Lalaurette, 2002: Verification of precipitation forecasts over the Alpine region using a high-density observing network. Weather Forecasting, 17, 238-249.

Choi, W., S.J. Kim, P.F. Rasmussen, and A.R. Moore, 2009: Use of the North American regional reanalysis for hydrological modelling in Manitoba. Canadian Water Resources, Journal 34 (1), 17-36.

Christensen, J.H., T.R. Carter, M. Rummukainen, and G. Amanatidis, 2007: Evaluating the performance and utility of regional climate models: the PRUDENCE project. Climatic Change, 81(Suppl 1), 1-6.

Christensen, N., and D.P. Lettenmaier, 2007: A multimodel ensemble approach to assessment of climate change impacts on the hydrology and water resources of the Colorado River basin. Hydrology and Earth System Sciences, 11, 1417-1434.

Chu, T.C., 2002: Selecting plant location via a fuzzy TOPSIS approach. The International Journal of Advanced Manufacturing Technology, 20(11), 859-864.

Chung, E.S., and G.S. Lee, 2009: Identification of spatial ranking of hydrological vulnerability using multi-criteria decision making techniques: Case study of Korea. Water Resources Management, 23, 2395-2416.

Crozier, L., R.W. Zabel, and A.H. Hamlet, 2007: Predicting differential effects of climate change at the population level with life-cycle models of spring Chinook salmon. Global Change Biology, 14, 236-249.

Daly, C., 2006: Guidelines for assessing the suitability of spatial climate data sets. International Journal of Climatology, 26: 707-721, doi:10.1002/joc.1322.

Daly, C., W.P. Gibson, G.H. Taylor, G.L. Johnson, and P. Pasteris, 2002: A knowledge-based approach to the statistical mapping of climate. Climate Research, 22, 99-113.

Daly, C., M. Halbleib, J.I. Smith, W.P. Gibson, M.K. Doggett, G.H. Taylor, J. Curtis, and P.P. Pasteris, 2008: Physiographically sensitive mapping of climatological

temperature and precipitation across the conterminous United States. International Journal of Climatology, 28, 2031-2064.

Daly, C., E.H. Helmer, and M. Quinones, 2003: Mapping the climate of Puerto Rico, Vieques, and Culebra. International Journal of Climatology, 23, 1359-1381.

Daly, C., R.P. Neilson, and D.L. Phillips, 1994: A statistical-topographic model for mapping climatological precipitation over mountainous terrain. Journal of Applied Meteorology, 33, 140-158.

Deque, M., D.P. Rowell, D. Luthi, F. Giorgi, J.H. Christensen, B. Rockel, D. Jacob, E. Kjellstrom, M. Castro, and B. van den Hurk, 2007: An intercomparison of regional climate simulations for Europe: assessing uncertainties in model projections. Climatic Change, 81, 53-70.

Dibike, Y. B., and P. Coulibaly, 2006: Temporal neural networks for downscaling climate variability and extremes. Neural Networks, 19, 135-144.

Diez, E., C. Primo, J.A. Garcia-Moya, J.M. Gutierrez, and B. Orfila, 2005: Statistical and dynamical downscaling of precipitation over Spain from DEMETER seasonal forecasts. Tellus Series, A 57, 409-423.

Donaldson, R.J., R.M. Dyer, and M.J. Kraus, 1975: An objective evaluator of techniques for predicting severe weather events. In: Preprints, Ninth Conference on Severe Local Storms, Norman, Oklahoma. American Meteorological Society, 321-326.

Eum, H.-I., Y.B. Dibike, T. Prowse, and B. Bonsal, 2014: Inter-comparison of high-resolution gridded climate data sets and their implication on hydrological model simulation over the Athabasca Watershed, Canada. Hydrological Processes, 28, 4250-4271.

Eum, H.-I., P. Gachon, R. Laprise, and T. Ouarda, 2012: Evaluation of regional climate model simulations versus gridded observed and regional reanalysis products using a combined weighting scheme. Climate Dynamics, 38, 1433-1457.

Eum, H.-I., Y.-O. Kim, and R.N. Palmer, 2011: Optimal drought management using sampling stochastic dynamic programming with a hedging rule. Journal of Water Resources Planning and Management, 137(1), 113-122.

Eum, H.-I., and S.P. Simonovic, 2012: Assessment on variability of extreme climate events for the Upper Thames River basin in Canada. Hydrological Processes 26, 485-499, doi:10.1002/hyp.8145.

Eum, H.-I., S.P. Simonovic, and Y.-O. Kim, 2010: Climate change impact assessment using k-nearest neighbor weather generator: Case study of the Nakdong River basin in Korea. Journal of Hydrologic Engineering, 15(10), 772-785.

Fasbender, D., and T.B.M.J. Ouarda, 2010: Spatial Bayesian model for statistical downscaling of AOGCM to minimum and maximum daily temperatures. Journal of Climate, 23, 5222-5242, doi:10.1175/2010JCLI3415.1.

Fernández, J., and J. Sáenz, 2003: Improved field reconstruction with the analog method: Searching the CCA space. Climate Research, 24, 199-213.

Finley, J.P., 1884: Tornado predictions. American Meteorological Journal, 1, 85-88.

Fowler, H.J., S. Blenkinsop, and C. Tebaldi, 2007: Linking climate change modelling to impacts studies: Recent advances in downscaling techniques for hydrological modelling. International Journal of Climatology, 27, 1547-1578.

Gilbert, G.K., 1884: Finley's tornado predictions. American Meteorological Journal, 1, 166-172.

Goodess, C.M., C. Anagnostopoulou, A. Bardossy, C. Frei, C. Harpham, M.R. Haylock, Y. Hundecha, P. Maheras, J. Ribalaygua, J. Schmidli, T. Schmith, K. Tolika, R. Tomozeiu, and R.L. Wilby, 2012: An intercomparison of statistical downscaling methods for Europe and European regions—assessing their performance with respect to extreme temperature and precipitation events. Climate Research Unit Research Publication, 11 (CRU RP11).

Gutmann, E., T. Pruitt, M.P. Clark, L. Brekke, J.R. Arnold, D.A. Raff, and R.M. Rasmussen, 2014: An intercomparison of statistical downscaling methods used for water resources assessments in the United States. Water Resources Research, 50, 7167-7186, doi:10.1002/2014WR015559.

Hanson, R.T., L.E. Flint, A.L. Flint, M.D. Dettinger, C.C. Faunt, D. Cayan, and W. Schmid, 2012: A method for physically based model analysis of conjunctive use in response to potential climate changes. Water Resources Research, 48, W00L08, doi:10.1029/2011WR010774.

Hay, L., J. LaFontaine, and S. Markstrom, 2014: Evaluation of statistically downscaled GCM output as input for hydrological and stream temperature simulation in the Apalachicola-Chattahoochee-Flint River Basin (1961-1999). Earth Interaction, 18, 1-32, doi:10.1175/2013EI000554.1.

Haylock, M.R., G.C. Cawley, C. Harpham, R.L. Wilby, and C.M. Goodess, 2006: Downscaling heavy precipitation over the UK: a comparison of dynamical and statistical methods and their future scenarios. International Journal of Climatology, 26, 1397-1415.

Hempel, S., K. Frieler, L. Warszawski, J. Schewe, and F. Piontek, 2013: A trend-preserving bias correction—the ISI-MIP approach. Earth System Dynamics, 4(2), 219-236.

Hidalgo, H., M. Dettinger, and D. Cayan, 2008: Downscaling with constructed analogues:

Daily precipitation and temperature fields over the United States, Rep. CEC-500-2007 -123, Calif. Energy Comm., PIER Energy-Related Environ. Res., Sacramento, Calif.

Hong, K.O., M.S. Suh, D.K. Rha, D.H. Chang, C. Kim, and M.K. Kim, 2007: Estimation of high resolution gridded temperature using GIS and PRISM. Atmosphere, 17, 255-268 (in Korean).

Hopkinson, R.F., D.W. McKeney, E.J. Milewska, M.F. Hutchinson, P. Papadopol, and L.A. Vincent, 2011: Impact of aligning climatological day on gridding daily maximum–minimum temperature and precipitation over Canada. Journal of Applied Meteorology and Climatology, 50, 1654-1665.

Hunter, R.D., and R.K. Meetemeyer, 2005: Climatologically aided mapping of daily precipitation and temperature. Journal of Applied Meteorology, 44, 1501-1510.

Hutchinson, M.F., 2004: ANUSPLIN version 4.3. Centre for Resource and Environmental Studies. Australian National University Canberra. [Available online at http://fennerschool.anu.edu.au/ publications/software/anusplin.php.]

Hutchinson, M.F., D.W. McKenney, K. Lawrence, J.H. Pedlar, R.F. Hopkinson, E. Milewska, and P. Papadopol, 2009: Development and testing of Canada-wide interpolated spatial models of daily minimum–maximum temperature and precipitation for 1961–2003. Journal of Applied Meteorology and Climatology, 48, 725-741.

Hwang, S., and W.D. Graham, 2013: Development and comparative evaluation of a stochastic analog method to downscale daily GCM precipitation, Hydrology and Earth System Sciences Discussion, 10, 2141-2181, doi:10.5194/hessd-10-2141-2013.

Hwang, C.l., and K. Yoon, 1981: Multiple Attribute Decision Making: Methods and Applications. New York, Springer-Verlag.

Jenkins, G., and J. Lowe, 2003: Handling uncertainties in the UKCIP02 scenarios of climate change. Hadley Centre Technical Note, 44, Exeter.

Johansson, B., and D. Chen, 2005: Estimation of areal precipitation for runoff modelling using wind data: a case study in Sweden. Climate Research, 29, 53-61.

Jun, K.-S., E.-S. Chung, Y.-G. Kim, and Y. Kim, 2013: A fuzzy multi-criteria approach to flood risk vulnerability in South Korea by considering climate change impacts. Expert Systems with Applications, 40, 1003-1013.

Karl, T.R., N. Nicholls, and A. Ghazi, 1999: CLIVAR/GCOS/WMO workshop on indices and indicators for climate extremes. Workshop summary. Climatic Change, 42, 3-7.

Kay, A.L., H.N. Davies, V.A. Bell, and R.G. Jones, 2009: Comparison of uncertainty sources for climate change impacts: Flood frequency in England. Climatic Change, 92, 41-63.

Kharin, V.V., F.W. Zwiers, X. Zhang, and G.C. Hegerl, 2007: Changes in temperature and precipitation extremes in the IPCC ensemble of global coupled model simulations. Journal of Climate, 20, 1419-1444.

Kim, Y., and E.-S. Chung, 2014: An index-based robust decision making framework for watershed management in a changing climate. Science of the Total Environment, 473-474, 88-102.

Kim, J.P., W.-S. Lee, H. Cho, and G. Kim, 2014: Estimation of high resolution daily precipitation using a modified PRSM model. Journal of the Korean Society of Civil Engineers, 34(4), 1139-1150.

Lapen, D.R., and H.N. Hayhoe, 2003: Spatial analysis of seasonal and annual temperature and precipitation normals in Southern Ontario, Canada. Journal of Great Lakes Research, 29(4), 529-544.

Lee, W.-S., J.A. Chun, and K. Kang, 2014: Development and application of GIS-based PRISM integration through a plugin approach. Journal of Hydrology, 513, 58-67.

Lee, G., K.-S. Jun, and E.-S. Chung, 2013: Integrated multi-criteria flood vulnerability approach using fuzzy TOPSIS and Delphi technique. Natural Hazards and Earth System Sciences, 13, 1293-1312.

Li, H., J. Sheffield, and E.F. Wood, 2010: Bias correction of monthly precipitation and temperature fields from Intergovernmental Panel on Climate Change AR4 models using equidistant quantile matching. Journal of Geophysical Research, 115, D10101, doi:10.1029/2009JD012882.

Lorenz, E.N., 1969: Atmospheric Predictability as Revealed by Naturally Occurring Analogues. Journal of the Atmospheric Sciences, 26, 636-646

Maloney, E.D., S.J. Camargo, E. Chang, B.C. Colle, R. Fu, K.L. Geil, Q. Hu, X. Jiang, N. Johnson, K.B. Karnauskas, J. Kinter, B. Kirtman, S. Kumar, B. Langenbrunner, K. Lombardo, L.N. Long, A. Mariotti, J.E. Meyerson, K.C. Mo, J.D. Neelin, Z. Pan, R. Seager, Y. Serra, A. Seth, J. Sheffield, J. Stroeve, J. Thibeault, S.-P.Xie, C. Wang, B. Wyman, and M. Zhao, 2014: North American Climate in CMIP5 experiments: Part III: Assessment of twenty-first century projections. Journal of Climate, 27, 2230-2270.

Maraun, D., 2013: Bias correction, quantile mapping, and downscaling: Revisiting the inflation issue. Journal of Climate, 26(6), 2137-2143.

Maurer, E.P., and H.G. Hidalgo, 2008: Utility of daily vs. monthly large-scale climate data: an intercomparison of two statistical downscaling methods. Hydrology and Earth System Sciences, 12, 551-563.

Maurer, E.P., H.G. Hidalgo, and T. Das, 2010: The utility of daily large-scale climate data in the assessment of climate change impacts on daily streamflow in California, Hydrology and Earth System Sciences, 14, 1125-1138, doi:10.5194/hess-14-1125-2010.

Maurer, E.P., and D.W. Pierce, 2014: Bias correction can modify climate model simulated precipitation changes without adverse effect on the ensemble mean. Hydrology and Earth System Sciences, 18(3), 915-925.

Maurer, E.P., A.W. Wood, J.C. Adam, D.P. Lettenmaier, and B. Nijssen, 2002: A long-term hydrologically based data set of land surface fluxes and states for the conterminous United States. Journal of Climate, 15, 3237-3251.

Mearns, L.O., R. Arritt, S. Biner, M.S. Bukovsky, S. McGinnis, S. Sain, D. Caya, J. Correia Jr., D. Flory, and W. Gutowski, 2012. The North American Regional Climate Change Assessment Program: Overview of Phase I Results, Bulletin of the American Meteorological Society, 93(9), 1337-1362.

Mesinger, F., G. Dimego, E. Kalnay, K. Mitchell, P.C. Shafran, W. Ebisuzaki, D. Jovic, J. Woollen, E. Rogers, E.H. Berbery, M.B. Ek, Y. Fan, R. Grumbine, W. Higgins, H. Li, Y. Lin, G. Manikin, D. Parrish, and W. Shi, 2006: North American Regional Reanalysis. Bulletin of the American Meteorological Society, 87, 343-360.

Miller, W.P., G.M. DeRosa, S. Gangopadhyay, and J.B. Valdes, 2013: Predicting regime shifts in flow of the Gunnison River under changing climate conditions. Water Resources Research, 49, 2966-2974, doi:10.1002/wrcr.20215.

Min, S.-K., X. Zhang, F.W. Zwiers, and G.C. Hegerl, 2011: Human contribution to more-intense precipitation extremes. Nature, 470, 378-381.

Mizuta, R., K. Oouchi, H. Yoshimura, A. Noda, K. Katayama, S. Yukimoto, M. Hosaka, S. Kusunoki, H. Kawai, and M. Nakagawa, 2006: 20-km-mesh global climate simulations using JMA-GSM model—mean climate states. Journal of the Meteorological Society of Japan, 84,165-185.

Monk, W.A., D.L. Peters, A.R. Curry, and D.J. Baird, 2011: Quantifying trends in indicator hydroecological variables for regime-based groups of Canadian rivers. Hydrological Processes, 25 (19), 3086-3100.

Murdock, T.Q., A.J. Cannon, and S.R. Sobie, 2013: Statistical downscaling of future climate projections. Pacific Climate Impacts Consortium (PCIC) Report (No.KM170-12-1236).

Murphy, A.H., 1997: The Economic Value of Weather and Climate Forecasts. Cambridge University Press, Cambridge, 19-74.

Neilsen, D., G. Duke, B. Taylor, J. Byrne, S. Kienzle, and T. Van der Gulik, 2010:

Development and verification of daily gridded climate surfaces in the Okanagan basin of British Columbia. Canadian Water Resources Journal, 35(21), 131-154.

Nicholas, R.E., and D.S. Battisti, 2012: Empirical downscaling of high-resolution regional precipitation from large-scale reanalysis fields. Journal of Applied Meteorology and Climatology, 51, 100-114, doi:10.1175/JAMC-D-11-04.1.

Olsson, J., C. Uvo, and K. Jinno, 2001: Statistical atmospheric downscaling of short-term extreme rainfall by neural networks. Physics and Chemistry of the Earth, 26B, 695-700.

Osborn, H.B., 1984: Estimating precipitation in mountainous regions. Journal of Hydraulic Engineering, 110, 1859-1863.

Petrik, R., M. Baldauf, H. Schlunze, and A. Gassmann, 2011: Validation of a mesoscale weather prediction model using subdomain budgets. Tellus seriries A. Dynamic Meteorology and Oceanography, 63 (4), 707-726.

Phillips, D.L., J. Dolph, and D. Marks, 1992: A comparison of geostatistical procedures for spatial analysis of precipitation in mountainous terrain. Agricultural and Forest Meteorology, 58, 119-141.

Rinke, A., P. Marbaix, and K. Dethloff, 2004: Internal variability in Arctic regional climate simulations: case study for the SHEBA year. Climate Research, 27, 197-209.

Roman, D.C., R.M. Vogel, and G.E. Schwarz, 2012: Regional regression models of watershed suspended-sediment discharge for the eastern United States. Journal of Hydrology, 472-473, 53-62.

Saha, S., S. Moorthi, H.-L. Pan, X. Wu, J. Wang, S. Nadiga, P. Tripp, R. Kistler, J. Woollen, D. Behringer, H. Liu, D. Stokes, R. Grumbine, G. Gayno, J. Wang, Y.-T. Hou, H.-Y. Chuang, H.M.H. Juang, J. Sela, M. Iredell, R. Treadon, D. Kleist, P.V. Delst, D. Keyser, J. Derber, M. Ek, J. Meng, H. Wei, R. Yang, S. Lord, H. van den Dool, A. Kumar, W. Wang, C. Long, M. Chelliah, Y. Xue, B. Huang, J.-K. Schemm, W. Ebisuzaki, R. Lin, P. Xie, M. Chen, S. Zhou, W. Higgins, C.-Z. Zou, Q. Liu, Y. Chen, Y. Han, L. Cucurull, R.W. Reynolds, G. Rutledge, and M. Goldberg, 2010: The NCEP climate forecast system reanalysis. Bulletin of the American Meteorological Society, 91(8), 1015-1057.

Segui, P.Q., A. Rebies, E. Martin, F. Habets, and J. Boe, 2010: Comparison of three downscaling methods in simulating the impact of climate change on the hydrology of Mediterranean basins. Journal of Hydrology, 383, 111-124.

Shin, S.C., M.K. Kim, M.S. Suh, D.K. Rha, D.H. Jang, C.S. Kim, W.S. Lee, and Y.H. Kim,

2008: Estimation of high resolution gridded precipitation using GIS and PRISM. Atmospheres, 18, 71-81 (in Korean).

Sillmann, J., V. Kharin, X. Zhang, F. Zwiers, and D. Bronaugh, 2013: Climate extremes indices in the CMIP5 multimodel ensemble: Part 1. Model evaluation in the present climate. Journal of Geophysical Research: Atmospheres, 118(4), 1716-1733.

Stoner, A., K. Hayhoe, and X. Yang, 2013: An asynchronous regional regression model for statistical downscaling of daily climate variables. International Journal of Climatology, 33, 2473-2494, doi:10.1002/joc.3603.

Swets, J.A., 1986: Form of empirical ROCs in discrimination and diagnostic tasks: implications for theory and measurement of performance. Psychological Bulletin, 99, 181-198.

Tebaldi, C., K. Hayhoe, J.M. Arblaster, and G.A. Meehl, 2006: Going to the extremes. Climatic Change, 79, 185-211.

Thornton, P., S.W. Running, and M.A. White, 1997: Generating surfaces of daily meteorological variables over large regions of complex terrain. Journal of Hydrology, 190, 214-251.

Thrasher, B., E.P. Maurer, C. McKellar, and P. Duffy, 2012: Technical Note: Bias correcting climate model simulated daily temperature extremes with quantile mapping, Hydrology and Earth System Sciences, 16, 3309-3314, doi:10.5194/hess-16-3309-2012.

Tikhonov, A.N., A.V. Goncharsky, V.V. Stepanov, and A.G. Yagola, 1995: Numerical Methods for the Solution of Ill-Posed Problems, Kluwer Academic Publishers.

Timbal, B., A. Dufour, and B. McAvaney, 2003: An estimate of future climate change for western France using a statistical downscaling technique. Climate Dynamics, 20, 807-823.

van den Dool, H.M., 1994: Searching for analogues, how long must one wait? Tellus Ser. A, 46, 314-324.

Vano J. A., B. Nijssen, and D.P. Letenmaier, 2015: Seasonal hydrologic responses to climate change in the Pacific Northwest. Water Resources Research, 51, 1959-1976.

Vogel, R.M., I. Wilson, and C. Daly, 1999: Regional regression models of annual streamflow for the United States. Journal of Irrigation and drainage Engineering, 125, 148-157.

Wang X., and B. Peng, 2015: Determining the value of the port transport waters: Based on improved TOPSIS model by multiple regression weighting. Ocean & Coastal

Management, 107, 37-45.

Wernberg, T., D.A. Smale, F. Tuya, M.S. Thomsen, T.J. Langlois, T. de Bettignies, S. Bennett, and C.S. Rousseaux, 2012: An extreme climatic event alters marine ecosystem structure in a global biodiversity hotspot. Nature Climate Change, 3 (1), 78-82.

Werner, A.T., M.A. Schnorbus, R.R. Shrestha, and H.D. Eckstrand, 2013: Spatial and temporal change in the hydro-climatology of the Canadian portion of the Columbia River basin under multiple emissions scenarios. Atmosphere-Ocean, 51(4), 357-379.

Wilby, R.L., and I. Harris, 2006: A framework for assessing uncertainties in climate change impacts: Low-flow scenarios for the River Thames, UK. Water Resources Research, 42, W02419, doi:10.1029/2005WR004065.

Wilby, R.L., L.E. Hay, W.J. Gutowski, R.W. Arritt, E.S. Takle, Z. Pan, G.H. Leavesley, and M.P. Clark, 2000: Hydrological responses to dynamically and statistically downscaled climate model output. Geophysical Research Letters, 27(8), 1199-1202, doi:10.1029/ 1999GL006078.

Wilby, R., T. Wigley, D. Conway, P. Jones, B. Hewitson, J. Main, and D. Wilks, 1998: Statistical downscaling of general circulation model output: A comparison of methods. Water Resource Research, 34, 2995-3008, doi:10.1029/98WR02577.

Wilks, D.S., 1995: Statistical Methods in the Atmospheric Sciences: An Introduction. Academic Press, San Diego.

Wood, A.W., L.R. Leung, V. Sridhar, and D.P. Lettenmaier, 2004: Hydrologic implications of dynamical and statistical approaches to downscaling climate model outputs. Climatic Change, 62, 189-216.

Wu, T., and Y. Li, 2013: Spatial interpolation of temperature in the United States using residual kriging. Applied Geography, 44, 112-120.

Zhang, X., L. Alexander, G.C. Hegerl, P. Jones, A.K. Tank, T.C. Peterson, B. Trewin, and F.W. Zwiers, 2011: Indices for monitoring changes in extremes based on daily temperature and precipitation data. Climate Change, 2(6), 851-870, doi:10.1002/wcc.147.

Zhang, X., G. Hegerl, F. Zwiers, and J. Kenyon, 2005: Avoiding inhomogeneity in percentile-based indices of temperature extremes. Journal of Climate, 18, 1641-1651.

Zhou, Y.G., J.J. Wen, and D.W. Chen, 2012: Study on the competitive and layout of commercial pedestrian streets' business forms though IEW & TOPSIS- two comparative cases in Hangzhou. Journal of Zhejiang University Science, 39 (6), 724-731.

Research Report 2015–05

High-resolution gridded data generation and performance assessment of multiple statistical downscaling methods for South Korea

Hyung–Il Eum

APCC
APEC CLIMATE CENTER

APEC Climate Center
12 Centum 7-ro, Haeundae-gu, Busan 48058, Republic of Korea
Tel: +82-51-745-3900 Fax: +82-51-745-3949

www.apcc21.org

9 791156 981060 93550
ISBN 979-11-5698-106-0